heig-vd
Haute Ecole d'Ingénierie et de Gestion
du Canton de Vaud

Laboratoire de thermique
industrielle et système

Institut de génie thermique

CO_2 Hydrate Slurry

GRS 32/08

Final Report

Abstract

CO_2 hydrate slurry is one of the newly developed secondary cooling fluids based on CO_2, an inoffensive gas in combination with water under suitable pressure and temperature conditions. A new CO_2 hydrate slurry production system was built and tested. Based on previous studies, a comprehensive kinetic study of CO_2 hydrates formation and growth was conducted. Solid mass fraction of CO_2 hydrate slurry was determinated. The experimental results show that besides pressure and temperature, density and apparent viscosity change can also be good indicators of the hydrate formation. The results have shown that hydrate creation through the heat exchanger by super cooling of the saturated CO_2 solution is feasible. Continuous CO_2 hydrate slurry formation and dissociation by heat exchanger was proved to be feasible. The pressure drop of CO_2 hydrate slurry with different solid mass fraction on heat exchanger as function of steady flow mean velocities were presented and verified. The stability of CO_2 hydrate slurry was examined. CO_2 hydrate slurry displayed very good stability at steady state during 11.5 hours running test. Longer stability period should be expected if the running conditions are maintained.

Jin HU[1], Osmann SARI[1], Cyril MAHMED[1], Raffaele CEREGHETTI[1], Paul HOMSY[2]

[1] Institute of Thermal Engineering, University of Applied Sciences of Western Switzerland

Avenue des Sports 20, 1400 Yverdon-les-Bains, Vaud, Switzerland

[2] Nestec, Avenue Nestlé 55, 1800 Vevey, Switzerland

*Osmann.sari@heig-vd.ch

Yverdon-les-Bains, July 2010

Table of Contents

1. Summary

CO_2 hydrate slurry is one of the newly developed secondary cooling fluids based on CO_2, an inoffensive gas in combination with water under suitable pressure and temperature conditions. A new CO_2 hydrate slurry production system was built and tested. Based on previous studies, a comprehensive kinetic study of CO_2 hydrates formation and growth was conducted. Solid mass fraction of CO_2 hydrate slurry was determinated. The experimental results show that besides pressure and temperature, density and apparent viscosity change can also be good indicators of the hydrate formation. The results have shown that hydrate creation through the heat exchanger by super cooling of the saturated CO_2 solution is feasible. Continuous CO_2 hydrate slurry formation and dissociation by heat exchanger was proved to be feasible. The pressure drop of CO_2 hydrate slurry with different solid mass fraction on heat exchanger as function of steady flow mean velocities were presented and verified. The stability of CO_2 hydrate slurry was examined. CO_2 hydrate slurry displayed very good stability at steady state during 11.5 hours running test. Longer stability period should be expected if the running conditions are maintained.

2. Nomenclature

Symbol	Signification	Units
A	Kinetic factor accounts for the mechanism of attachment of hydrate building units to nucleus and for the kind of nucleation	--
A_p	Surface area	m^2
A_s	Area of this surface or interface	m^2
a	Lattice parameter of a unit cell of Structure I hydrate	m
a_w	Area occupied by a water molecule on the substrate surface or at the solution/gas interface	m^2
B	Dimensionless thermodynamic parameter	--
B'	Thermodynamic parameter	--
C	Actual concentration (m^{-3}) of dissolved gas in the aqueous solution	mol/kg
C_0	Concentration of nucleation sites in the system	--
C_e	Concentration of dissolved gas at phase equilibrium between hydrate and solution	mol/kg
C_p	Specific heat	J/kg.K
C_{p_c}	Specific heat of the cold fluid	J/kg.K
C_{p_h}	Specific heat of the hot fluid	J/kg.K
C_{p_w}	Specific heat of water	J/kg.K
C_{par}	Concentration of nucleation-active particles in the solution	--
C_s	CO_2 solubility in water	(mol/k/g)
C_t	Time-dependent gas concentration	mol/kg
c	A numerical shape factor	--
$c_{p,h}$	Constant-pressure heat capacity per hydrate building unit in the hydrate crystal	J/kg.K
$c_{p,w}$	Constant-pressure heat capacity per water molecule in the solution	J/kg.K
$c_{p,gg}$	Constant-pressure heat capacity per gas molecule in the gas phase	J/kg.K
D	Diffusion coefficient of dissolved gas in the aqueous solution	--
D_c	Outer diameter of pipes wherein coolant flows	m
D_{ef}	Effective diffusion coefficient characterizing the random events of transfer of hydrate building units across the nucleus/solution interface.	--

D_h	Hydraulic diameter	m
D_i	Inner diameter of the pipes wherein the CO_2 hydrate slurry flows	m
D_o	Outer diameter of the pipes wherein the CO_2 hydrate slurry flows	m
D'	Inner diameter of pipes wherein coolant flows	m
d_h	Diameter of the hydrate building unit	m
f*	Attachment frequency	--
f_e^*	Factor with a value equal or often close to that of f* at $\Delta\mu$=0	--
G_{sys}	Gibbs free energy of the system	J/mol
h	Heat transfer coefficient	$W/m^2.K$
h_c	Heat transfer coefficient of coolant	$W/m^2.K$
h_{Hy}	Heat transfer coefficient of hydrate slurry	$W/m^2.K$
J	Nucleation rate	--
k	Boltzmann constant	--
L	Length of the tube	m
M	molar mass	g/mol
M_{CO_2}	Molar mass of CO_2	kg/mol
M_{H_2O}	molar mass of water	g/mol
$M_{CO2,\ solution}$	Molar mass of CO_2 solution	g/mol
$\dot{m}$	Mass flow rate	kg/s
$\dot{m}_c$	Mass flow rates of the cold fluid	kg/s
$\dot{m}_h$	Mass flow rates of the hot fluid	kg/s
N_a	Number of nucleation-active centers on such a particle, on the substrate or at the solution/ gas interface	--
N_g	Number of gas molecules in the solution	--
N_w	Number of water molecules in the solution	--
N_0	Avogadro constant	--
n_g	Number of gas molecules per unit cell of the hydrate crystal lattice	--
n_w	Hydration number in CO_2 gas hydrate, $5.75 \leq n_w \leq 7.67$	--
n*	Nucleus size	m
P	Pressure	Pa
$P_e(T)$	Phase equilibrium pressure	Pa
Pr	Prandtl number of the fluid	--

P'	Temperature ratio parameter	--
$\dot{Q}$	Heat transfer rate	W
R	Temperature ratio parameter	--
Re_{Dh}	Reynolds number of the flow	--
r_c	Critical radius at which G_{sys} reaches its maximum value	--
S	Independent kinetic parameter	--
s_h	Entropy of hydrate	J/K
s_w	Entropy of water	J/K
s_{gg}	Entropy of gas	J/K
T	Temperature	K/°C
T_c	Critical temperature	K/°C
T_e	Equilibrium temperature	K/°C
T_{ci}	Temperatures of cold fluid at position inlet	(K/°C)
T_{co}	temperatures of cold fluid at position outlet	K/°C
T_{hi}	Temperatures of hot fluid at position inlet	K/°C
T_{ho}	Temperatures of hot fluid at position outlet	K/°C
T^*	Reference temperature	K/°C
t_s	Time at which the solution becomes supersaturated	s
U	Overall heat transfer coefficient	$W/m^2.K$
V	Volume of the solution	m^3
$V_{CO_2Solution}$	CO_2 solution molar volume	m^3/mol
V_l	Water molar volume	m^3/mol
ν_c	Critical volume	m^3
ν_h	Volume of a building unit in the hydrate crystal	m^3
ν_w	Volume of a water molecule in the solution	m^3
ν_{ef}	Effective molecular volume	m^3
ν_{cell}	Volume of hydrate crystal cell	m^3
W	Work to form a hydrate cluster constituted of n building units	J/mol
W^*	Nucleation work	J/mol
x	Molar fraction	--

x_{CO_2}	Molar fraction of CO_2	--
x_{H_2O}	Molar fraction of water	--
$x_{CO_2 hydrate}$	Hydrate solid mass fraction in the hydrate slurry	--
$x_{CO_2}^{hydrate}$	Molar fraction of CO_2 in the CO_2 hydrate	--
z	Zeldovich factor, z≈0.01-1	--
γ	Activity coefficient of dissolved gas	--
λ	Thermal conductivity of the fluid (W/m.K)	W/m.K
μ	Dynamic viscosity of the fluid (Pa. s)	Pa.s
$\mu_{h,0}$	Reference chemical potentials depending only on T	--
$\mu_{w,0}$	Reference chemical potentials depending only on T	--
μ_{gg}	Chemical potential of a gas molecule in the gas phase	--
$\mu_{gg,0}$	Reference chemical potentials depending only on T	--
μ_h^*	Reference chemical potentials depending only on P	--
μ_w^*	Reference chemical potentials depending only on P	--
μ_{gg}^*	Reference chemical potentials depending only on P	--
$\mu_{gs}^{\bullet}$	Reference chemical potential, a function of P and T only	--
μ_w	Chemical potentials of the water molecules in the aqueous solution	--
μ_{gs}	Chemical potentials of the gas molecules in the aqueous solution	--
μ_{hs}	Chemical potential of a hydrate building unit in the solution	--
φ	Fugacity coefficient of the gas	--
η	Occupancy of cavities in Structure I hydrate (%)	%
ε	Sticking coefficient of hydrate building units to the nucleus surface, $\varepsilon \leq 1$	--
$\rho_{hydrate}$	CO_2 hydrate density	kg/m^3
$\rho_{Hyslurry}$	CO_2 hydrate slurry density	kg/m^3
$\rho_{CO_2 Solution}$	Saturated CO_2 solution density (kg/m^3)	kg/m^3
ψ	Number between 0 and 1	--
θ	Hydrate/substrate “wetting” angles with values from 0° to 180°	--
θ_0	Angles with values from 0° to 180°	--

σ	Specific surface energy of the hydrate/ solution interface	J/m^2
σ_{ef}	Effective specific surface energy	J/m^2
σ_{hg}	Specific surface energies of the hydrate/gas interfaces	J/m^2
σ_{hs}	Specific surface energies of the hydrate/substrate interfaces	J/m^2
σ_{sg}	Specific surface energies of the solution/gas interfaces	J/m^2
σ_{ss}	Specific surface energies of the solution/substrate	J/m^2
τ	Time constant for establishment of the solution/gas chemical equilibrium	--
$\Delta c_{p,e}$	Differences between the heat capacities of the old and the new phase at $T=T_e$	--
Δh_e	Experimentally accessible enthalpy or latent heat (per hydrate building unit) of dissociation of hydrate crystal into gaseous phase and liquid water at T=Te	--
Δs	Hydrate dissociation entropy per hydrate building unit, i.e. the entropy change in the transfer at the given P and T of one gas molecule from the hydrate crystal into the gas phase.	--
Δs_e	Differences between the entropies of the old and the new phase at $T=T_e$,	--
ΔT	Under cooling	--
ΔT_{LM}	Log mean temperature difference	K
$\Delta\mu$	Chemical potential of a building unit (one gas molecule and n_w water molecules) in hydrate crystal	--
$\Delta\mu_t$	Time-dependent supersaturation	--
Nu_{Dh}	Nusselt number of the flow	--
HON	Homogeneous nucleation	--
HEN	Heterogeneous nucleation	--

3. Introduction

The impact of synthetic refrigerants on the environment as well as the legal safety obligations drive the refrigeration industry to seek for new ways for completely phasing out greenhouse gases or for decreasing their charge in miscellaneous installations. One of the possible solutions could be to reduce the quantity of these primary refrigerants by utilizing secondary refrigerants. The principle of such technology consists in using two different loops. The primary loop, of reduced dimensions and working with a classical refrigerant is set in an engine room. It exchanges heat with the fluid running in the secondary loop, which is responsible for the cold energy distribution. Therefore, this technology leads to a reduction of the total amount of classical refrigerant.

Ice slurry as a kind of secondary refrigerants has been used over a decade (Bel et al., 1999; Tanino et al., 2001; Ayel et al., 2003; Matsumoto et al., 2004). However, application of ice-slurry is limited due to high cost of ice-slurry generator and power limitation. Concerning air-conditioning systems, in recent years, the tetra-n-butylammonium bromide (TBAB) semi-clathrate hydrate seems to be a good secondary refrigerant candidate for this application field. Since TBAB hydrate slurry are more environmentally friendly than CFC refrigerant and present a positive melting temperature. Moreover, it can be formed under atmosphere. (Tanasawa and Takao, 2002; Ogoshi and Takao, 2004; Oyama et al., 2005; Darbouret et al., 2005; Lin et al., 2008).

CO_2 hydrate slurry is one of the secondary fluids based on CO_2, an inoffensive gas. Note that here CO_2 can be recovered from existing industrial processes (for example fermentation) and is not specially produced for the purpose. This suggests that the process could contribute to replace polluting fluids which will be prohibited from 2014 on. Consequently, a high potential market is arising.

CO_2 hydrate slurry is obtained by the combination of water and CO_2 (gas or liquid) under certain conditions of temperature and pressure. The process of hydrates ($CO_2 \cdot n_w H_2O$) formation is described by the equation (1).

$$CO_2 + n_w H_2O \longleftrightarrow CO_2 \cdot n_w H_2O \quad (1)$$

Hydrates are ice-like solids that form when:

a sufficient amount of water is present

a hydrate former is present

the right combination of temperature and pressure (hydrate formation is favoured by low temperature and high pressure)

Hydrates are non-stoichiometric crystalline compounds formed by cavities of “host” water molecules. A stable hydrate forms without all of the cages being occupied. The degree of saturation (the number occupied cages) is a function of the temperature and the pressure. Under certain pressure and temperature conditions they are strongly hydrogen bonded with a small guest molecule hydrate structure. There are two types of CO_2 hydrate, namely hydrate I with structure I and hydrate II with structure II respectively. Hydrate I is the most common structure occurring in CO_2 hydrates. Hereafter, only hydrate I will be referred to as CO_2 hydrate.

As the formation of gas hydrate is an exothermic equilibrium process. The dissociation of gas hydrate is an endothermic equilibrium process. To use this endothermic process is to benefit from the latent heat of fusion of the CO2 hydrate phase change. First, CO2 clathrate hydrates can be utilized for refrigeration applications, such as cold storage since their large heat of melting was confirmed by various authors (Skovborg and Rasmussen 1994; Anderson, 2003; Uchida et al., 1995, 1996; Udachin et al., 2001; Fournaison et al., 2004; Marinhas et al., 2006). Since CO_2 hydrate phase change temperature is above the freezing point of water (Hironori et al., 2001; Circone et al., 2003), the use of CO_2 hydrate energy is clearly relevant for the field of air conditioning. Moreover, CO2 hydrate slurries are fluid enough to flow easily through the secondary refrigerant loop (Marinhas et al., 2006; Hu et al., 2008; Delahaye et al., 2008) up to operating solid concentrations (30% or more at lab scale). Nevertheless, in order to be eligible for industry applications, the hydrate slurry must satisfy three major criteria: sufficient solid fraction to provide a large cold source and stable temperature levels during hydrate dissociation; stable enough for the pumping and transportation; appropriate flowing conditions of slurry to have efficient heat exchanges;

Previous research work focused on the investigation of physical and thermal properties of hydrate slurry (Sari et al., 2007; Hu et al., 2008). To better utilize CO_2 hydrate slurry as newly developed secondary refrigerant, a pilot CO_2 slurry production system was newly built.

The major objectives of the project are to create CO_2 hydrate slurry directly by super cooling saturated CO_2 solution through heat exchanger and study the performance of heat exchanger in order to approach practical industrial systems; study the continuous formation and dissociation process of CO_2 hydrate slurry; study the stability, flow behaviours and heat transfer of CO_2 hydrate slurry. In order to improve the design and operation of a heat exchanger/generator of CO_2 hydrate slurry and present a clear modelling target to tackle the complex phenomenon of hydrate formation and hydrate growth, the state-of-the-art of kinetics study of CO_2 hydrates formation and growth seems also very necessary and important.

4. Kinetic Study of CO_2 Hydrates Formation and Growth

This study is part of global project aiming to use CO_2 hydrate slurries as secondary refrigerants in indirect refrigeration applications and, in particular, to improve the design and operation of a heat exchanger/generator of these types of slurries.

This will involve the following sub-objectives:

- Driving force for crystallization of CO_2 gas hydrate,
- Nucleation of CO_2 gas hydrate.

4.1 Driving Force for Crystallization of CO_2 Gas Hydrate

We consider a three-phase system of a one component gas, an aqueous solution of the gas and a crystalline hydrate of the gas (Fig. 1). The gas phase is treated as one-component, because the partial pressure of water vapour in it is often negligible at the hydrate crystallization temperatures. The system is held at fixed pressure P and temperature T; and the hydrate phase is considered as resulting from the following precipitation ‘‘reaction’’ occurring in the solution [Sloan, 1998]

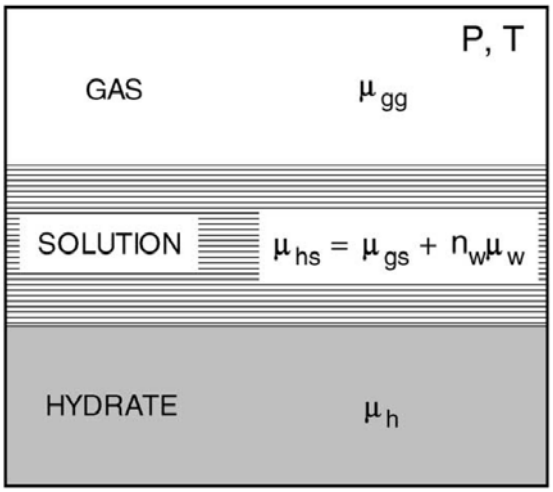

Fig.1: Three-phase system of one-component gas, aqueous solution of the gas and gas hydrate

The relation (1) implies that the crystallization of the hydrate in the solution is analogous to the precipitation of inorganic salts in aqueous solutions. Indeed, one molecule CO_2 of the dissolved gas and n_w water molecules of the solution form one building unit $CO_2 \cdot n_w H_2O$ of the hydrate crystal.

For stoichiometric CO_2 gas hydrates of the cubic structures sI , the hydration number n_w has values between 5.75 and 7.67 (Teng, H., et al 1996). The cubic structures sI is shown in the figure 2.

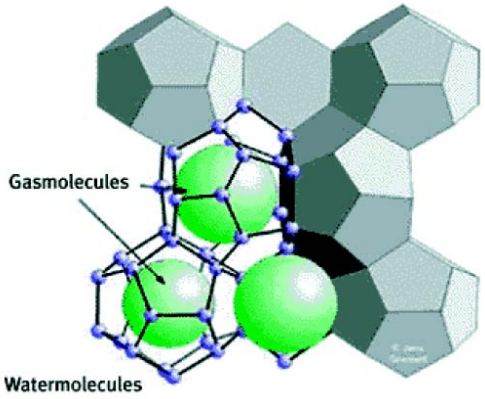

Fig.2: The structure of sI hydrate

μ_{gs} and μ_w are the chemical potentials of the gas and water molecules in the aqueous solution, respectively (Fig. 1). According to the thermodynamic relation between chemical potentials in reaction equilibria [Denbigh, 1971] and Eq. (1), for the chemical potential μ_{hs} of a hydrate building unit in the solution we shall have [Makogon, 1997]

$$\mu_{hs} = \mu_{gs} + n_w \cdot \mu_w \qquad (2)$$

By definition [Kashchiev, 2000], the driving force for new phase formation is the difference between the chemical potentials of the old and the new phases. This difference is called supersaturation and is commonly denoted by $\Delta\mu$: Hence, if $\Delta\mu$ is the chemical potential of a building unit (one gas molecule and n_w water molecules) in the hydrate crystal (Fig. 1), the supersaturation $\Delta\mu$ in hydrate formation will be given by

$$\Delta\mu = \mu_{gs} + n_w \mu_w - \mu_h \tag{3}$$

because μ_{hs} fromEq. (2) and μ_h are the chemical potentials of the old and the new phases, respectively. Nucleation and/or growth of hydrate crystals are possible only when $\Delta\mu > 0$: then $\mu_{hs} > \mu_h$ [Makogon, 1997] and the solution is supersaturated. If $\Delta\mu = 0$; the solution is saturated and the system is in phase equilibrium: then $\mu_{hs} = \mu_h$ and the dissolved and crystalline hydrate phases can coexist. When $\Delta\mu < 0$; the solution is undersaturated: as then $\mu_{hs} < \mu_h$; hydrate crystals cannot nucleate in the solution, and existing ones are subject to dissolution.

Thus, while $\Delta\mu$ is the driving force for hydrate formation, $-\Delta\mu$ is the driving force for hydrate dissolution.

The general Eq. (3) allows expressing $\Delta\mu$ in terms of the actual concentration C (m^{-3}) of dissolved gas in the aqueous solution. As known from thermodynamics [Firoozabadi, 1999]

$$\mu_{gs}(P,T,C) = \mu^{\bullet}_{gs}(P,T) + k \cdot T \cdot \ln\left[\frac{\gamma(P,T,C)\cdot N_g}{N_g + N_w}\right] \tag{4}$$

where $\mu^{\bullet}_{gs}$, a function of P and T only, is a reference chemical potential; k is the Boltzmann constant; γ is the activity coefficient of dissolved gas, and N_g and N_w are the number of gas and water molecules in the solution, respectively. Denoting by V for the volume of the solution, and by ν_w the volume of a water molecule in it, we have $N_w \approx \frac{V}{\nu_w}$, N_w is total number of water molecules; because $N_w >> N_g$, N_g is total number of gas molecules: Taking into account $N_g = CV$, we can rewrite Eq. (4) in the form

$$\begin{aligned}\mu_{gs}(P,T,C) &= \mu^{\bullet}_{gs}(P,T) + k \cdot T \cdot \ln\left[\frac{\gamma(P,T,C)\cdot C \cdot V}{N_w}\right] \\ &= \mu^{*}_{gs}(P,T) + k \cdot T \cdot \ln\left[\gamma(P,T,C)\cdot \nu_w \cdot C\right]\end{aligned} \tag{5}$$

Employing this expression in Eq. (3), recalling that n_w is a function of P and T [Sloan, 1998] and accounting that μ_w and μ_h are virtually C-independent leads to the following formula:

$$\Delta\mu = k \cdot T \cdot \ln\left[\gamma(P,T,C) \cdot \nu_w \cdot C\right] + \mu^*_{gs}(P,T) + n_w(P,T) \cdot \mu_w(P,T) - \mu_h(P,T) \quad (6)$$

This general equation gives the dependence of $\Delta\mu$ on C in crystallization of gas hydrates in aqueous solutions of one-component gases. Adopting the convention [Firoozabadi, 1999] of gas as a solute allows using the approximation $\gamma \approx 1$ because of the relatively low solubility of most gases in water and the substance behaves as if it were ideal, which is known as Raoult's Law.

Eq. (6) shows that if we use approximation of $\gamma = 1$, $\Delta\mu$ increases logarithmically with C.

This means that the concrete conditions of dissolution of the gas into the aqueous phase are of prime importance for supersaturating the system.

If the system is at equilibrium, then the chemical potential of the component i must be the same in the liquid solution and in the vapor above it. That is,

$$\mu_{gs} = \mu_{gg} \quad (7)$$

where μ_{gg} is the chemical potential of a gas molecule in the gas phase (Fig. 1). Eq. (7) implies that in the case of solution/gas chemical equilibrium the right-hand side of Eq. (4) or (5) is equal to μ_{gg}: Hence, in this case we can replace the first two summands on the right-hand side of Eq. (6) by μ_{gg} in order to eliminate the gas concentration C andobtain $\Delta\mu$ in the form:

$$\Delta\mu = \mu_{gg}(P,T) + n_w(P,T) \cdot \mu_w(P,T) - \mu_h(P,T) \quad (8)$$

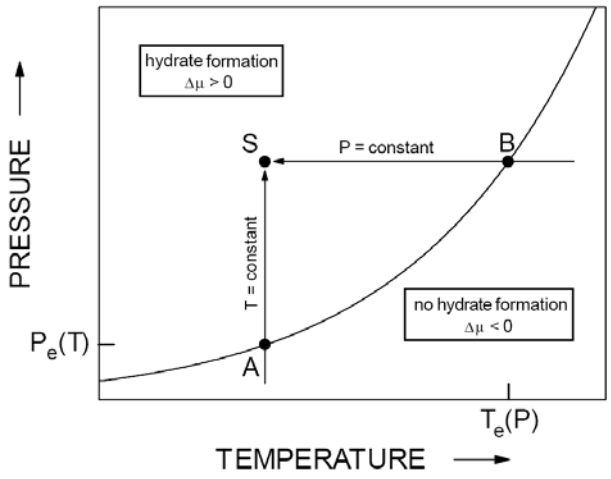

Fig.3: Gas/solution/hydrate phase diagram: for P; T values on curve AB the solution is saturated ($\Delta\mu = 0$) and can coexist with the hydrate; for P; T values above curve AB the solution is supersaturated ($\Delta\mu > 0$) and hydrate crystallization is possible; for P;T values below curve AB the solution is undersaturated ($\Delta\mu < 0$) and no hydrate crystallization can occur. The arrows from points A and B to point S symbolize solution supersaturating in isothermal and isobaric regime, respectively.

This general formula reveals that in the case of solution/gas chemical equilibrium $\Delta\mu$ depends on P and T only.

Now consider the two important regimes of isothermal and isobaric variation of $\Delta\mu$.

Isothermal Regime

In this regime $\Delta\mu$ is varied by changing P at constant T: This is illustrated in Fig. 3 by the arrow passing through point A and ending at point S which represents the state of the system at given values of P and T. From thermodynamics [Firoozabadi, 1999], for this regime we can write

$$\mu_{gg}(P,T) = \mu_{gg,0}(T) + k \cdot T \cdot \ln\left[\varphi(P,T) \cdot P\right] \tag{9}$$

$$\mu_{w}(P,T) = \mu_{w,0}(T) + \int_0^P \nu_{w}(P',T) \cdot dP' \tag{10}$$

$$\mu_{h}(P,T) = \mu_{h,0}(T) + \int_0^P \nu_{h}(P',T) \cdot dP' \tag{11}$$

Where φ is the fugacity coefficient of the gas, which can be obtained by using the Peng-Robinson equation of state for CO_2 gas. $\nu_w(m^3)$ is the volume of a water molecule in the solution; ν_h is volume of a building unit in the hydrate crystal. $\mu_{gg,0}$, $\mu_{w,0}$, $\mu_{h,0}$ are reference chemical potentials depending only on T. If we substitute Eqs (9), (10) and (11) into Eq (8)

$$\begin{aligned}\Delta\mu = {} & \mu_{gg,0}(T) + k \cdot T \cdot \ln\left[\varphi(P,T) \cdot P\right] + n_w(P,T) \cdot \left(\mu_{w,0}(T) + \int_0^P \nu_{w}(P',T) \cdot dP'\right) \\ & - \mu_{h,0}(T) - \int_0^P \nu_{h}(P',T) \cdot dP'\end{aligned} \tag{12a}$$

$$\begin{aligned}\Delta\mu = {} & \mu_{gg,0}(T) + k \cdot T \cdot \ln\left[\varphi(P,T)P\right] \cdot \mu_{w,0}(T) + n_w(P,T) \cdot \int_0^P \nu_{w}(P',T) \cdot dP' \\ & - \mu_{h,0}(T) - \int_0^P \nu_{h}(P',T) dP'\end{aligned} \tag{12b}$$

As already noted, the phase equilibrium between solution and hydrate is characterized by $\Delta\mu$=0. At the chosen temperature T, the supersaturation becomes zero at the equilibrium (more accurately, phase equilibrium) pressure Pe (T) corresponding to point A in Fig. 3. The *Pe* (T) function is illustrated by the curve in this figure and can be obtained from the expression

$$\begin{aligned}0 = {} & \mu_{gg,0}(T) + k \cdot T \cdot \ln\left[\varphi(P_e,T) \cdot P_e\right] + n_w(P_e,T) \cdot \mu_{w,0}(T) \\ & + n_w(P_e,T) \cdot \int_0^{P_e} \nu_{w}(P',T) \cdot dP' - \mu_{h,0}(T) - \int_0^{P_e} \nu_{w} \cdot (P',T) dP'\end{aligned} \tag{13}$$

$$\mu_{gg,0}(T)-\mu_{h,0}(T)=\int_0^{P_e}\nu_h(P',T)\cdot dP'-k\cdot T\cdot\ln\left[\varphi(P_e,T)P_e\right] - n_w(P_e,T)\cdot\mu_{w,0}(T)-n_w(P_e,T)\cdot\int_0^{P_e}\nu_w(P',T)\cdot dP' \tag{14}$$

This expression in Eq (14) allows elimination of the reference chemical potentials $\mu_{gg,0}$ and $\mu_{h,0}$ in Eq. (12)

$$\Delta\mu=k\cdot T\cdot\ln\left[\varphi(P,T)\cdot P\right]+n_w(P,T)\cdot\mu_{w,0}(T)+n_w(P,T)\cdot\int_0^P\nu_w(P',T)\cdot dP' -\int_0^P\nu_h(P',T)\cdot dP'+\int_0^{P_e}\nu_h(P',T)\cdot dP'-k\cdot T\cdot\ln\left[\varphi(P_e,T)\cdot P_e\right]-n_w(P_e,T)\cdot\mu_{w,0}(T) -n_w(P_e,T)\cdot\int_0^{P_e}\nu_w(P',T)\cdot dP'$$

$$\Delta\mu=k\cdot T\cdot\ln\left[\varphi(P,T)\cdot P\right]-k\cdot T\cdot\ln\left[\varphi(P_e,T)\cdot P_e\right]+ \left[n_w(P,T)-n_w(P_e,T)\right]\cdot\mu_{w,0}(T)+n_w(P,T)\cdot\int_0^P\nu_w(P',T)\cdot dP' -n_w(P_e,T)\cdot\int_0^{P_e}\nu_w(P',T)\cdot dP'+\int_0^{P_e}\nu_h(P',T)\cdot dP'-\int_0^P\nu_h(P',T)\cdot dP'$$

$$\Delta\mu=k\cdot T\cdot\ln\left(\frac{\varphi(P,T)\cdot P}{\varphi(P_e,T)\cdot P_e}\right)+\left[n_w(P,T)-n_w(P_e,T)\right]\cdot\mu_{w,0}(T) +n_w(P,T)\cdot\int_0^P\nu_w(P',T)\cdot dP'-n_w(P_e,T)\cdot\int_0^{P_e}\nu_w(P',T)\cdot dP'-\int_{p_e}^P\nu_h(P',T)\cdot dP' \tag{15}$$

This is the general formula for $\Delta\mu$ in isothermal regime provided the solution is in chemical Equilibrium with the gas phase.

Isobaric Regime

In this regime $\Delta\mu$ is varied by changing T at constant P: This is schematized in Fig. 3 by the arrow heading through point B to point S. From thermodynamics [Firoozabadi, 1999], in isobaric regime μ_{gg},μ_w,μ_h are given by

$$\mu_{gg}(P,T)=\mu_{gg}^*(P)-\int_{T^*}^T s_{gg}(P,T')\cdot dT' \tag{16}$$

$$\mu_w(P,T)=\mu_w^*(P)-\int_{T^*}^T s_w(P,T')\cdot dT' \tag{17}$$

$$\mu_h(P,T)=\mu_h^*(P)-\int_{T^*}^T s_h(P,T')\cdot dT' \tag{18}$$

Here S_{gg}, S_w *and* S_h are the entropies per gas molecule in the gas phase, per water molecule in the solution and per hydrate building unit in the hydrate crystal, respectively. $\mu^*_{gg}, \mu^*_w, \mu^*_h$.

are reference chemical potentials depending only on P; and T* is a reference temperature. Using the above equations in the general expression for $\Delta\mu$ in Eq. (8), results in

$$\begin{aligned}\Delta\mu = {} & \mu^*_{gg}(P) + n_w(P,T)\cdot\mu^*_w(P) - \mu^*_h(P) \\ & - n_w(P,T)\cdot\int_{T^*}^{T} s_w(P,T')\cdot dT' - \int_{T^*}^{T}\left[s_{gg}(P,T') - s_h(P,T')\right]\cdot dT'\end{aligned} \tag{19}$$

At the chosen pressure P, there exists a temperature *Te* (P) at which the solution and the hydrate phase can coexist, because then $\Delta\mu$=0. This temperature is therefore the equilibrium (more accurately, phase equilibrium) temperature of the system. It corresponds to point B in Fig. 3 and is the solution of the equation.

$$\begin{aligned}0 = {} & \mu^*_{gg}(P) + n_w(P,T_e)\cdot\mu^*_w(P) - \mu^*_h(P) - n_w(P,T'_e)\cdot\int_{T^*}^{T_e} s_w(P,T')\cdot dT' \\ & - \int_{T^*}^{T_e}\left[s_{gg}(P,T') - s_h(P,T')\right]\cdot dT'\end{aligned} \tag{20}$$

$$\begin{aligned}\mu^*_{gg}(P) - \mu^*_h(P) = {} & n_w(P,T_e)\cdot\int_{T^*}^{T_e} s_w(P,T')\cdot dT' \\ & + \int_{T^*}^{T_e}\left[s_{gg}(P,T') - s_h(P,T')\right]\cdot dT' - n_w(P,T_e)\cdot\mu^*_w(P)\end{aligned} \tag{21}$$

Employing Eq. (21) to eliminate μ^*_{gg}, $\mu^*_h(P)$ from E q. (19), we get:

$$\begin{aligned}\Delta\mu = {} & \left[n_w(P,T) - n_w(P,T_e)\right]\cdot\mu^*_w(P) - n_w(P,T)\cdot\int_{T^*}^{T} s_w(P,T')\cdot dT' \\ & + n_w(P,T_e)\cdot\int_{T^*}^{T_e} s_w(P,T')\cdot dT' + \int_{T}^{T_e}\left[s_{gg}(P,T') - s_h(P,T')\right]\cdot dT'\end{aligned} \tag{22}$$

This is the general formula for $\Delta\mu$ in isobaric regime when there exists chemical equilibrium between the solution and the gas phase.

A general expression is derived for the supersaturation for crystallization of one-component gas hydrates in aqueous solutions. The supersaturation is the driving force of the process, since it represents the difference between the chemical potentials of a hydrate building unit in the solution and in the hydrate crystal.

Absence of Chemical Equilibrium between Solution and Gas Phase

We now consider the case when the pressure and the temperature of the system are fixed, but there is no chemical equilibrium between the solution and the gas phase. In this case, the actual concentration of gas in the solution varies with time t [Natarajan, 1993 and Natarajan *et*

al, 1994], because the condition for chemical equilibrium, Eq. (7) is not fulfilled. According to Eq. (6), this means that the supersaturation itself is also a function of time.

Denoting by $\Delta\mu_t$ and C_t these time-dependent supersaturation and gas concentration, Eq. (6) is in the form of:

$$\begin{aligned}\Delta\mu_t &= k\cdot T\cdot \ln\left[\gamma(P,T,C_t)\cdot \nu_w\cdot C_t\right]+\mu^*_{gs}(P,T)\\ &\quad + n_w(P,T)\cdot\mu_w(P,T)-\mu_h(P,T)\end{aligned} \tag{23}$$

To make physically more revealing this general formula for the variable supersaturation during hydrate crystallization in the absence of solution/gas chemical equilibrium it is convenient to relate C_t to the equilibrium gas concentration C by means of the expression

$$C_t = C\cdot x(t) \tag{24}$$

The dimensionless function $x(t)$ takes into account the concrete kinetics of reaching the solution/gas chemical equilibrium at the given pressure and temperature and satisfies the condition for $t\to\infty$, $x(t)\to 1$. Under non-equilibrium conditions, $C_t < C$.

A model $x(t)$ dependence characterizing initially gas-free water is,

$$x(t) = 1 - e^{\frac{-t}{\tau}} \tag{25}$$

where τ is the time constant for establishment of the solution/gas chemical equilibrium [Natarajan, 1993].

Therefore, Eq. (23) should be:

$$\begin{aligned}\Delta\mu_t &= k\cdot T\cdot \ln\left[\gamma(P,T,C_t)\cdot \nu_w\cdot C\cdot x(t)\right]+\mu^*_{gs}(P,T)\\ &\quad + n_w(P,T)\cdot\mu_w(P,T)-\mu_h(P,T)\end{aligned} \tag{26}$$

$$\begin{aligned}\Delta\mu_t &= k\cdot T\cdot \ln\left[\gamma(P,T,C_t)\cdot \nu_w\cdot C\right]+k\cdot T\cdot\ln\left[x(t)\right]\\ &\quad + \mu^*_{gs}(P,T)+n_w(P,T)\cdot\mu_w(P,T)-\mu_h(P,T)\end{aligned} \tag{27}$$

using the approximation $\gamma(P,T,C_t)\approx\gamma(P,T,C)$,

$$\begin{aligned}\Delta\mu_t &= k\cdot T\cdot \ln\left[\gamma(P,T,C)\cdot \nu_w\cdot C\right]+k\cdot T\cdot\ln\left[x(t)\right]+\mu^*_{gs}(P,T)\\ &\quad + n_w(P,T)\cdot\mu_w(P,T)-\mu_h(P,T)\end{aligned} \tag{28}$$

Recall that equation (6) gives the dependence of $\Delta\mu$ on C in crystallization of gas hydrates in aqueous solutions of one-component gases. Employing Eq. (6) into Eq. (28), yields the general formula.

$$\Delta\mu_t = \Delta\mu + k\cdot T\cdot\ln\left[x(t)\right] \tag{29}$$

Here $\Delta\mu$ is specified by Eq. (6) and is the time independent supersaturation corresponding to established chemical equilibrium between the solution and the gas phase at the given pressure and temperature of the system. Hence, in general, in Eq. (29) we can use $\Delta\mu$ from Eq. (8) in order to present $\Delta\mu_t$ as:

$$\Delta\mu_t = \mu_{gg}(P,T) + n_w(P,T)\cdot\mu_w(P,T) - \mu_h(P,T) + k\cdot T\cdot\ln[x(t)] \tag{30}$$

In particular, as shown, in Eq. (29) we can employ any of the formulae for $\Delta\mu$ to determine $\Delta\mu_t$ in isothermal or isobaric regime.

Isothermal Approximation Based on Isothermal Regime

Assume

$$n_w \approx n_w(P_e,T)$$

$$\nu_w \approx \nu_w(P_e,T)$$

$$\nu_h \approx \nu_h(P_e,T)$$

These relations imply negligible pressure dependence of the hydration number and of the compressibility of the aqueous and hydrate phases for P close enough to P_e. Their use in Eq. (15) results in

$$\Delta\mu = k\cdot T\cdot\ln\left(\frac{\varphi(P,T)\cdot P}{\varphi(P_e,T)\cdot P_e}\right) + \Delta\nu_e\cdot(P-P_e) \tag{31}$$

$$\Delta\nu_e(T) = n_w(P_e,T)\cdot\nu_w(P_e,T) - \nu_h(P_e,T) \tag{32}$$

If n_g is the number of gas molecules per unit cell of the hydrate crystal lattice, this cell contains n_g building units (the n_g value may differ from that corresponding to the stoichiometric hydrate crystal). Hence, denoting by ν_{cell} (m^3) the volume of this cell, we can calculate ν_h by using the relation:

$$\nu_{cell} = n_g \times \nu_h \tag{33}$$

Combining Eqs. (32) and (33) leads to the formula:

$$\Delta\nu_e = n_w\cdot\nu_w - \frac{\nu_{cell}}{n_g} \tag{34}$$

In isothermal regime, if we assume:

$$\varphi(P,T) \approx \exp(\frac{b \cdot P}{k \cdot T})$$

This relation gives the fugacity coefficient φ in terms of the second virial coefficient b (m^3) of the gas contacting the solution [Denbigh, 1971]. This coefficient changes from negative to positive with increasing temperature. Values of b for some gases at T = 273.2 K are presented in Table 1.

Table 1 : Hydrate crystal structure[a] and values of hydration number n_w of stoichiometric hydrates crystal[a], number n_g of gas molecules per unit cell of stoichiometric hydrate crystal[a], volume v_h of hydrate building unit, volume difference Δv_c second viral coefficient b (at T = 273.2 K)[b] and effective volume v_{ef} (at T = 273.2 K) for various gases

Gas	Hydrate Structure	n_w	n_g	v_h (nm^3)	$-\Delta v_c$ (nm^3)	$-b$ (nm^3)	$-v_{ef}$ (nm^3)
Ar	sII	17/3	24	0.216	0.046	0.034	0.080
Kr	sII	17/3	24	0.216	0.046	0.099	0.145
N_2	sII	17/3	24	0.216	0.046	0.019	0.065
O_2	sII	17/3	24	0.216	0.046	0.036	0.082
CH_4	sI	23/4	8	0.216	0.044	0.086	0.130
Xe	sI	23/4	8	0.216	0.044	0.253	0.287
H_2S	sI	23/4	8	0.216	0.044	0.339	0.383
CO_2	sI	23/4	8	0.216	0.044	0.221	0.265
C_2H_6	sI	23/3	6	0.288	0.058	0.366	0.424
c-C_3H_4	sI	23/3	6	0.288	0.058	0.658	0.716
C_3H_8	sII	17	8	0.647	0.137	0.787	0.924
i-C_4H_{10}	sII	17	8	0.647	0.137	1.365	1.502

[a] According to Ref. [Sloan, 1998], p. 53

[b] Calculated from $\frac{b}{\nu_c} = 0.430 - 0.886(\frac{T_c}{T}) - 0.694(\frac{T_c}{T})^2 - 0.0375q(\frac{T_c}{T})^{4.5}$ (Ref. [Prausnitz *et al*, 1986], p. 126) where T_c and ν_c are the critical temperature and volume, respectively, and q=0 for Ar, Kr, N_2, O_2, CH_4, Xe, H_2S, CO_2 and c-C_3H_4.

The effective molecular volume ν_{ef} (m^3) is defined by :

$$\nu_{ef} = \Delta\nu_e + b \tag{35}$$

$$\Delta\nu_{ef} = \nu_e - b \tag{36}$$

Employing the above expressions for φ in Eq. (31) yields:

$$\Delta\mu = k \cdot T \cdot \ln(\frac{P}{P_e}) + \nu_{ef} \cdot (P - P_e) \tag{37}$$

Setting b = 0 in equation $\varphi(P,T) \approx \exp(\frac{b \cdot P}{k \cdot T})$, results in the ideal gas approximation φ=1. This approximation means that the hydrate-forming gas is treated as ideal, so that b=0.

Employing the above expression for φ in Eqs. (36) and (37) yields:

$$\Delta\mu = k \cdot T \cdot \ln(\frac{P}{P_e}) + \Delta\nu_e \cdot (P - P_e) \tag{38}$$

Isothermal Regime

Combing Eqs. (29) and (37) leads to the expression:

$$\Delta\mu_t = k \cdot T \cdot \ln(\frac{P}{P_e}) + \nu_{ef} \cdot (P - P_e) + k \cdot T \cdot \ln[x(t)] \tag{39}$$

To illustrate the time variation of the supersaturation for an initially gas-free liquid water brought into contact with a gas phase at time t = 0; we can substitute $x(t)$ from Eq. (25) into Eq. (39). This leads to the expression:

$$\Delta\mu_t = k \cdot T \cdot \ln\left(\frac{P}{P_e}\right) + \nu_{ef} \cdot (P - P_e) + k \cdot T \cdot \ln\left(1 - e^{\frac{-t}{\tau}}\right) \tag{40}$$

With formula 40, we can depict time dependence of $\Delta\mu_t$ for CO_2 hydrates at different temperature and pressure.

By using Eqs. (25). (29), we have equation:

$$\Delta\mu_t = \Delta\mu + k \cdot T \cdot \ln\left(1 - e^{\frac{-t}{\tau}}\right) \tag{41}$$

Setting $\Delta\mu_t(t_s)$ =0, t_s is the time at which the solution becomes supersaturated.

$$0 = \Delta\mu + k \cdot T \cdot \ln\left(1 - e^{\frac{-t}{\tau}}\right)$$

$$-\frac{\Delta\mu}{k\cdot T}=\ln\left(1-e^{\frac{-t}{\tau}}\right)$$

$$e^{\frac{-\Delta\mu}{k\cdot T}}=1-e^{\frac{-t_s}{\tau}}$$

$$e^{\frac{-t_s}{\tau}}=1-e^{\frac{-\Delta\mu}{k\cdot T}}$$

$$t_s=-\tau\cdot\ln\left(1-e^{\frac{-\Delta\mu}{kT}}\right) \tag{42}$$

As seen from this general expression, t_s depends not only on τ , but also on the equilibrium value $\Delta\mu$ of the supersaturation.

Isobaric Approximation Based on Isobaric Regime

Assume

$$n_w \approx n_w(P_e, T_e)$$

This approximation ignores the temperature dependence of the hydration number for T close enough to T_e and results in elimination of μ_w^* and T^* from Eq. (22). This equation thus becomes:

$$\Delta\mu=\int_T^{T_e}\Delta s(P,T')\cdot dT' \tag{43}$$

Where

$$\Delta s = s_{gg}(P,T)+n_w\cdot(P,T_e)\cdot s_w(P,T)-s_h(P,T) \tag{44}$$

is the hydrate dissociation entropy per hydrate building unit, i.e. the entropy change in the transfer at the given P and T of one gas molecule from the hydrate crystal into the gas phase and of n_w water molecules also from the hydrate crystal, but into the solution. Eq. (43) has the form of the known expression for $\Delta\mu$ in melt crystallization [Kashchiev, 2000] and allows calculation of the supersaturation from experimental data or theoretical formula for the temperature dependence of s_{gg}; s_w and s_h.

According to thermodynamics [Firoozabadi, 1999], the entropy s and the heat capacity c_p at constant pressure are related by $ds=\left(\frac{c_p}{T}\right)\cdot dT$. For that reason $\Delta\mu$ from Eq. (43) can be expressed in the following Taylor series about $T=T_e$ [Kashchiev, 2000].

$$\Delta\mu = \Delta s_e \cdot (T - T_e) - \left(\frac{\Delta c_{p,e}}{2 \cdot T_e}\right) \cdot (T - T_e)^2 - \left(\frac{T_e \cdot \Delta c'_{p,e} - \Delta c_{p,e}}{6 \cdot T_e^2}\right) \cdot (T - T_e)^3 - .... \quad (45)$$

Where Δs_e and $\Delta c_{p,e}$ are the differences between the entropies and the heat capacities of the old and the new phase at $T=T_e$, and $\Delta c'_{p,e} = \frac{d\Delta c_p}{dT}$ also at $T=T_e$.

To a first approximation of $n_w \approx n_w(P_e, T_e)$, in the case considered of hydrate crystallization we can write:

$$\Delta\mu = \Delta s_e \cdot \Delta T \quad (46)$$

$$\Delta T = T_e - T \quad (47)$$

ΔT is the undercooling, and the quantity Δs_e (J/K) is given by :

$$\Delta s_e = s_{gg}(P, T_e) + n_w(P, T_e) \cdot s_w(P, T_e) - s_h(P, T_e) \quad (48)$$

Δs_e is the value of Δs from Eq.(44) at the equilibrium temperature T_e.

According to Eq. (45) the $\Delta\mu(T)$ dependence is of the form:

$$\Delta\mu = \Delta s_e \cdot \Delta T - \left(\frac{\Delta c_{p,e}}{2T_e}\right) \cdot \Delta T^2 \quad (49)$$

where the heat capacity difference $\Delta c_{p,e}$ (J/K) is expressed as:

$$\Delta c_{p,e} = c_{p,gg}(P, T_e) + n_w(P, T_e) \cdot c_{p,w}(P, T_e) - c_{p,h}(P, T_e) \quad (50)$$

The constant-pressure heat capacities $c_{p,gg}$, $c_{p,w}$ and $c_{p,h}$ are, respectively, per gas molecule in the gas phase, per water molecule in the solution and per hydrate building unit (one gas molecule and n_w water molecules) in the hydrate crystal.

According to Eq.(46) , $\Delta\mu$ increases linearly with lowering T. Combining Eq.(46) and (47) we have

$$\Delta\mu = \Delta s_e \cdot (T_e - T) = \Delta s_e \cdot T_e - \Delta s_e \cdot T \quad (51)$$

From thermodynamics [Firoozabadi, 1999],

$$\Delta s_e \cdot T_e = \Delta h_e \quad (52)$$

where Δh_e (J) is the enthalpy or latent heat (per hydrate building unit) of dissociation of thehydrate crystal into gaseous phase and liquid water at $T = T_e$.

Isobaric Regime

In this regime we can employ Eq.(22), Eq.(43), Eq.(46) or Eq.(49) to express $\Delta\mu$ in Eq.(29) in the scope of the corresponding approximation.

$$\Delta\mu_t = \Delta s_e \cdot \Delta T + k \cdot T \cdot \ln\left(1 - e^{\frac{-t}{\tau}}\right) \tag{53}$$

The time t_s associated with the dependence given by Eq. (42)

Expressions for the supersaturation are obtained for solutions supersaturated in isothermal or isobaric regime. The results obtained are applied to the crystallization of hydrates of one-component gases.

4.2 Nucleation of CO_2 Gas Hydrate

4.2.1 Experimental Studies on Hydrate Nucleation

Hydrate formation is a phase change process and hence requires a supersaturation environment to take place. On account of this supersaturation, the Gibbs free energy of the gas dissolved in the liquid is greater than the respective Gibbs free energy of the hydrate, which favours the aggregation of water and gas molecules to form the hydrate. However, the separation of a new phase requires the formation of an interface, which is associated with a positive variation of the Gibbs free energy, as the molecules in the interfacial region always have more energy than those in the bulk phase. These two components of the Gibbs free energy of the system, G_{sys}, with opposite signs, depend on the size of the formed cluster. At the beginning of the process, the term related to the interfacial area, which grows with the square of the cluster radius, dominates, so that the formed clusters are more likely to decompose than to grow. Since the magnitude of the term associated with the bulk phase increases with the cube of the cluster radius, a minimum radius is eventually reached, known as the critical radius, r_c, at which G_{sys} reaches its maximum value. At this point, as $\frac{dG_{sys}}{dr} = 0$, the probabilities of cluster growth and decomposition are equal. For clusters with $r > r_c$, growth is always associated with a reduction in the Gibbs free energy of the system, being, thus, spontaneous.

In completely pure systems, free from any impurity in suspension, nucleation that occurs in the liquid bulk is said to be homogeneous. When pre-existing surfaces as those of particles in suspension or a wall or even between two phases promote nucleation due to a reduction in the Gibbs energy increase associated to the appearance of the new phase, the process is called heterogeneous nucleation. Considering that the complete removal of microparticles from a solution is a rather difficult task, in practice, heterogeneous nucleation is more commonly observed.

In heterogeneous nucleation, the contact angle between the hydrate and the pre-existing surface controls the reduction in the specific superficial energy of the solution–hydrate interface, which, in turn, decreases the amount of work required in the formation of the new phase. As a result, for heterogeneous nucleation, a smaller critical radius is verified. The

lower the contact angle, that is, the higher the affinity between the hydrate and the pre-existing surface, the more effective this effect will be (Kashchiev and Firoozabadi, 2002b).

In the specific case of hydrates of low-solubility gases, like hydrocarbons, since water is also scarcely soluble in these substances, the gas–liquid interface constitutes the most likely place for nucleation to occur, not only because of the reduced specific superficial energy between the hydrate and the solution, but mainly due to the fact that the highest concentrations of the molecules which compose the hydrate, and consequently the higher supersaturation conditions, are precisely found in this region. For carbon dioxide, nucleation at the gas–liquid interface started on the wall and the hydrate layer grew into the liquid bulk, which was confirmed by Takeya et al. (2000) with a high speed video camera.

In apparent contradiction to these results, Englezos et al. (1987a) reported the occurrence of nucleation everywhere in the liquid phase for different operating conditions during the formation of methane and ethane hydrates with distilled water in a stirred reactor, which was justified in terms of a uniform supersaturation of the liquid phase before nucleation due to stirring. Sloan (1998) states, however, that, for high stirring speeds, an apparent nucleation in the bulk liquid phase may simply be the result of a dispersion into the liquid bulk of clusters originally nucleated at the gas–liquid interface.

4.2.2 Hydrate Cluster Formation

The work to form a cluster of the new phase is a key parameter in the determination of the rate at which the phase is nucleated [Kashchiev, 2000]. As an example, this quantity has been successfully used to predict the location of the bubbles of the new vapour phase in two contacting immiscible liquids. When one of these liquids is superheated and the other is not, there are two possibilities for the formation of gaseous clusters, i.e. bubbles. One possibility is the bubble formation in the bulk of the superheated liquid. The other possibility is the formation of lens-shaped bubbles at the interface between the two immiscible liquids. Comparison of the measured and the theoretical temperatures for the onset of bubble nucleation shows that depending on the liquid/liquid and gas/liquid specific surface energies, the bubbles may come into being either in the superheated liquid or at the liquid/liquid interface.

In the formation of clusters in the bulk of the superheated liquid or at the interface between the superheated and the non-superheated liquid, there is a considerable success in verifying the nucleation theory with respect to the location of the cluster formation [Jarvis et al, 1975; Moore, 1956; Apfel, 1971]. Here we shall use a similar approach to examine the location of the hydrate clusters in the nucleation of one-component gas hydrates in aqueous solutions.

The work W (J) to form a hydrate cluster constituted of n building units can be determined by using the classical theory of nucleation. Application of the expression for W for three dimensional (3D) nucleation of one-component condensed phases [Kashchiev, 2000] to hydrate nucleation at a given supersaturation $\Delta\mu(J)$ yields

$$W(n) = -n_w \cdot \Delta\mu + c \cdot v_h^{2/3} \cdot \sigma_{ef} \cdot n_w^{2/3} \tag{54}$$

In this formula $\Delta\mu$ is a known function of the pressure P or the temperature T when it is varied isothermally or isobarically [Kashchiev & Firoozabadi, 2000a]. *c* is a numerical shape factor.

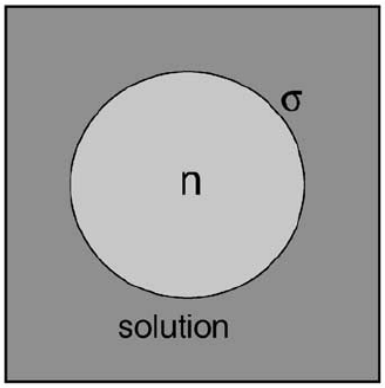

Fig. 4-a: Schematic of (a) spherical cluster of n building units in HON.

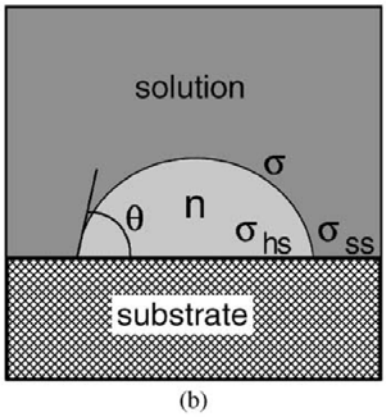

Fig. 4-b: Cap-shaped cluster of n building units in 3D HEN on a substrate

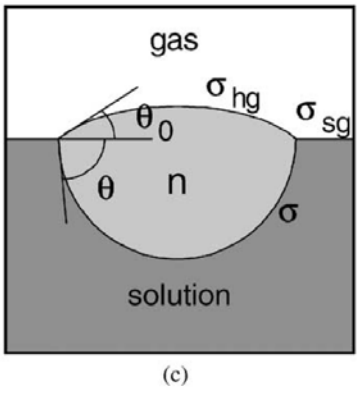

Fig. 4c: Lens-shaped cluster of n building units in 3D HEN at the solution/gas interface.

$C = (36 \cdot \pi)^{\frac{1}{3}}$ for spherical clusters (Fig. 4a) in homogeneous nucleation (HON) and for cap-shaped (Fig. 4b) or lens shaped (Fig. 4c) clusters in heterogeneous nucleation (HEN) on a solid substrate or at the interface between the solution and the gas phase. $v_h\,(\mathrm{m}^3)$ is the volume of a hydrate building unit (such unit comprises one gas molecule) and n_w water molecules [Kashchiev & Firoozabadi, 2000a], n_w being the hydration number), and σ_{ef} (J/m^2) is an effective specific surface energy. While for HON $\sigma_{ef} = \sigma$; for HEN $\sigma_{ef} < \sigma$; where σ (J/m^2) is the specific surface energy of the hydrate/ solution interface. σ_{ef} is treated as independent of pressure and temperature, because it is expected to remain nearly constant under typical conditions of hydrate crystallization.

In general, σ_{ef} is defined by [Kashchiev, 2000]

$$\sigma_{ef} = \psi \cdot \sigma \tag{55}$$

where the factor ψ is a number between 0 and 1. For instance, for cap-shaped clusters on a substrate (Fig. 4b) ψ reads [Kashchiev, 2000]

$$\psi = \left[\frac{1}{4} \cdot (2 + \cos\theta) \cdot (1 - \cos\theta)^2\right]^{\frac{1}{3}} \tag{56}$$

Where θ is the hydrate/substrate "wetting" angle with values from 0° to 180°. The Young equation [Adamson, 1982; Krotov & Rusanov, 1999]

$$\cos\theta = \frac{(\sigma_{ss} - \sigma_{hs})}{\sigma} \tag{57}$$

relates θ to σ_{ss} (J/m^2) and σ_{hs} (J/m^2) which are the specific surface energies of the solution/substrate and hydrate/substrate interfaces, respectively.

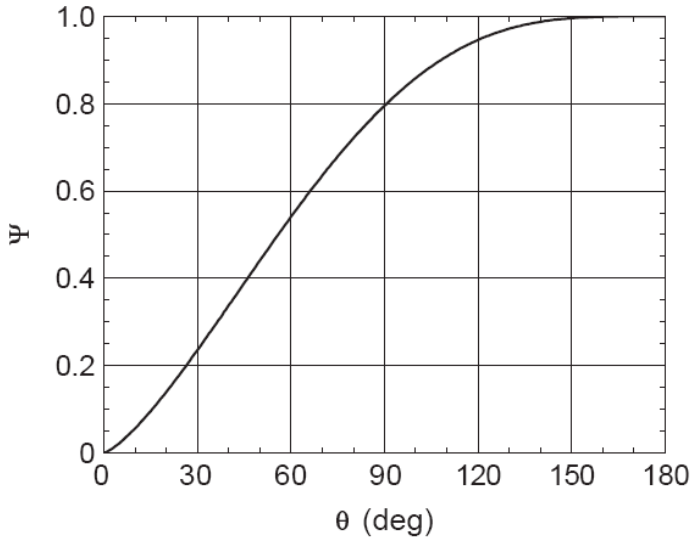

Fig.5: The factor ψ vs. the ''wetting'' angle θ according to equation (56)

Eq. (56) and its plot in Fig.5 show that at θ=0 (complete ‘‘wetting’’ of the substrate by the hydrate crystallite) ψ=0; at θ =180° (complete hydrate/substrate ‘‘non-wetting’’) $\psi = 1$;

Thus, energetically, HON appears as a limiting case of HEN with $\psi = 1$.

The same applies to lens shaped clusters at the solution/gas interface (Fig. 4c). The expression for ψ of the lens-shaped clusters is of the form [Kashchiev, 2000].

$$\psi = \left[\frac{1}{4} \cdot (2 + \cos\theta) \cdot (1 - \cos\theta)^2 + \frac{1}{4} \cdot (2 + \cos\theta_0) \cdot (1 - \cos\theta_0)^2 \cdot \left(\frac{\sin\theta}{\sin\theta_0} \right)^3 \right]^{\frac{1}{3}} \tag{58}$$

Here θ and θ_0 are angles between 0° and 180° and are obtained from [Kashchiev, 2000; Jarvis *et al*, 1975]

$$\cos\theta = \frac{(\sigma_{sg}^2 + \sigma^2 - \sigma_{hg}^2)}{2\sigma_{sg} \cdot \sigma} \tag{59}$$

$$\cos\theta_0 = \frac{\sigma_{sg}^2 - \sigma^2 + \sigma_{hg}^2}{2\sigma_{sg} \cdot \sigma_{hg}} \tag{60}$$

Where σ_{sg} (J/m^2) and σ_{hg} (J/m^2) are the specific surface energies of the solution/gas and hydrate/gas interfaces, respectively. From Eqs. (58)– (60), $\psi = 1$ when θ_0=0 and θ= 180°. This corresponds to spherical hydrate clusters just touching the solution/gas interface from the solution side. Thus, as already pointed out, when $\psi = 1$, HEN is energetically equivalent to HON.

Physically, the $\Delta\mu$ term in Eq. (54) represents the work gained upon assembling *n* hydrate building units into an *n*-sized hydrate cluster, because nucleation can occur only when $\Delta\mu$ > 0: The σ_{ef} term in this equation is the work done on creating the interface between the cluster and the ambient phase(s) (i.e. the solution in HON, the solution and the substrate or the gas phase in HEN).

4.2.3 Nucleus Size and Nucleation Work

As known from nucleation theory [Kashchiev, 2000], the position of the maximum of the *W(n)* function determines the number *n** of building units constituting the hydrate nucleus. Accordingly, the nucleation work *W* (J)* (which, physically, is the energy barrier to nucleation) is the value of *W* at *n* = *n**.

The general formulae for *n** and *W** for 3D nucleation of one-component condensed phases

[Kashchiev, 2000], are directly applicable to hydrate nucleation. Using them, we can write the expressions

$$n* = \frac{8 \cdot c^3 \cdot v_h^2 \cdot \sigma_{ef}^3}{27 \cdot \Delta\mu^3} \tag{61}$$

$$W* = \frac{4 \cdot c^3 \cdot v_h^2 \cdot \sigma_{ef}^3}{27 \cdot \Delta\mu^2} \tag{62}$$

which are readily obtained also from Eq. (54) and the extreme condition $\frac{dW}{dn} = 0$ at n=n*.

These expressions show explicitly how $n*$ and $W*$ decrease with increasing $\Delta\mu$ (i.e. with pressurizing or cooling the saturated solution) and/or with decreasing σ_{ef} (e.g., with improving the ‘‘wettability’’ of the substrate surface for the hydrate crystallites). With appropriate expressions for $\Delta\mu$ [Kashchiev & Firoozabadi, 2002a] Eqs. (61) and (62) are applicable to both HON ($\sigma_{ef} = \sigma$) and 3D HEN ($\sigma_{ef} < \sigma$) of hydrate crystallites under various conditions.

4.2.4 Nucleation Rate

We can now proceed with the determination of the nucleation rate J (m^{-3} s^{-1} or m^{-2} s^{-1}) of one component gas hydrates in aqueous solutions. According to nucleation theory, in the case of **stationary** nucleation of one-component phases J is given by the general expression [Kashchiev, 2000]

$$J = z \cdot f^* \cdot C_0 \cdot e^{\left(\frac{-W^*}{kT}\right)} \tag{63}$$

Where z≈0.01-1 is the so-called Zeldovich factor, f^* (s^{-1}) is the frequency of attachment of buliding units to the nucleus, and C_0 (m^{-3} or m^{-2}) is the concentration of nucleation sites in the system. For the 3D nucleation considered here z is related to $n*$ and $W*$ from Eqs. (61) and (62) by

$$z = \left(\frac{W^*}{3 \cdot \pi \cdot k \cdot T \cdot n^{*2}} \right)^{\frac{1}{2}} \tag{64}$$

The quantity C_0 depends essentially on the kind of nucleation: for hydrate nucleation in aqueous solutions there holds [Kashchiev, 2000]

$$C_0 = \frac{1}{v_w} \approx 3 \times 10^{28} m^{-3} \tag{65}$$

for HON,

$$C_0 = N_a \cdot C_{par} < 3 \times 10^{28} m^{-3} \tag{66}$$

for HEN on microscopically small nucleation active particles (crystallites, droplets or bubbles) present in insufficiently purified or degassed solutions,

$$C_0 \approx \frac{1}{a_w} \approx 8 \times 10^{18}\,m^{-2} \tag{67}$$

for HEN on solid substrates or at the solution/gas interface when these are free of nucleation-active centers (structural point defects, impurity molecules, adsorbed surfactants, etc.), and

$$C_0 = \frac{N_a}{A_s} < 8 \times 10^{18}\,m^{-2} \tag{68}$$

for HEN also on solid substrates or at the solution/gas interface, but with such centers on their surface.

In Eqs. (65) to (68), $a_w \approx \left(\frac{9 \cdot \pi \cdot v_w^2}{16}\right)^{\frac{1}{3}} \approx 0.12$ nm^2 is the area occupied by a water molecule on the substrate surface or at the solution/gas interface, A_s (m^2) is the area of this surface or interface, C_{par} (m^{-3}) is the concentration of nucleation-active particles in the solution, and N_a is the number of nucleation-active centers on such a particle, on the substrate or at the solution/ gas interface. Eqs. (65) to (68) merely express the fact that, physically, each water molecule or active centre provides a nucleation site in the solution, on the particle or substrate surface and at the solution/gas interface. When the molecules constituting the substrate surface or the solution/gas interface play the role of centers with equal nucleation activity, $Na \approx \frac{A_s}{a_w}$ and Eq. (68) passes into Eq. (67). Analogously, when all ‘‘surface’’ molecules of a particle with surface area A_p (m^2) play the same role, we have $Na \approx \frac{A_s}{a_w}$ and Eq. (66) becomes

$$C_0 \approx \frac{A_p \cdot C_{par}}{a_w} < 3 \times 10^{28}\,m^{-3} \tag{69}$$

For nucleation of one-component condensed phases in solutions the attachment frequency f^* is given by the general formula [Kashchiev, 2000]

$$f^* = f_e^* \cdot e^{\left(\frac{\Delta\mu}{k \cdot T}\right)} \tag{70}$$

In which f_e^* (s^{-1}) is a factor with a value equal or often close to that of f^* at $\Delta\mu = 0$. Hence, for hydrate nucleation in isothermal regime (then $\Delta\mu$ is specified by Eq. (71), f_e^* is approximately the frequency with which the hydrate building units would attach to the nucleus at $P=P_e$. In isobaric regime of hydrate nucleation $\Delta\mu$ is given by Eq. (72) and, to a certain approximation, f_e^* equals the frequency with which the hydrate nucleus would attach building units at $T=T_e$

$$\Delta\mu = k \cdot T \cdot \ln\left[\frac{\varphi(P,T)\cdot P}{\varphi(P_e,T)\cdot P_e}\right] + \Delta v_e \cdot (P - P_e) \tag{71}$$

$$\Delta\mu = \Delta s_e \cdot \Delta T \tag{72}$$

Here Δs_e (J/K) is the entropy (per hydrate building unit) of hydrate dissociation at $T=T_e$, and ΔT (K) is the undercooling defined by:

$$\Delta T = T_e - T \tag{73}$$

The Δs_e value can be obtained from the general relation $\Delta s_e = \frac{\Delta h_e}{T_e}$ in which Δh_e (J) is the experimentally accessible enthalpy or latent heat (per hydrate building unit) of dissociation of hydrate crystal into gaseous phase and liquid water at $T=T_e$.

In hydrate nucleation, as in other nucleation processes, f_e^* depends on the specifics of the kinetics of attachment of hydrate building units to the surface of the hydrate nucleus. For instance, when this attachment is governed by volume diffusion of dissolved gas towards a homogeneously formed nucleus, in isothermal regime f_e^* has the form [Kashchiev, 2000]

$$f_e^* = \varepsilon \cdot (4 \cdot \pi \cdot c)^{1/2} \cdot v_h^{1/3} \cdot D \cdot C_e \cdot n^{*1/3} \tag{74}$$

Similarly, for a nucleus formed homogeneously in isothermal regime, when attachment is governed by transfer of hydrate building units across the nucleus/solution interface, f_e^* reads [Kashchiev, 2000]:

$$f_e^* = \varepsilon \cdot \left(\frac{c \cdot v_h^{2/3}}{d_h}\right) \cdot D_{ef} \cdot C_e \cdot n^{*2/3} \tag{75}$$

In the above two equations $\varepsilon \leq 1$ is the sticking coefficient of hydrate building units to the nucleus surface, $d_h \approx \left(\frac{6 \cdot v_h}{\pi}\right)^{\frac{1}{3}}$ is the diameter of the hydrate building unit, D (m^2/s) is the diffusion coefficient of dissolved gas in the aqueous solution, D_{ef} (m^2/s) is an effective diffusion coefficient characterizing the random events of transfer of hydrate building units across the nucleus/solution interface, C_e (m^{-3}) is the concentration of dissolved gas at phase equilibrium between hydrate and solution (i.e. at $\Delta\mu = 0$), and n^* is the nucleus size determined by Eq. (61) at the existing supersaturation $\Delta\mu$.

Combining Eqs. (62) and (63) to (70), we find that the stationary rate of HON ($\sigma_{ef} = \sigma$) and 3D HEN($\sigma_{ef} < \sigma$) of one-component gas hydrate is given by

$$J = A \cdot e^{\Delta\mu / kT} \cdot \exp\left(\frac{-4 \cdot c^3 \cdot v_h^2 \cdot \sigma_{ef}^3}{27 \cdot k \cdot T \cdot \Delta\mu^2} \right) \tag{76}$$

The kinetic factor A ($m^{-3}s^{-1}$ or $m^{-2}s^{-1}$) in this formula accounts for the mechanism of attachment of hydrate building units to nucleus and for the kind of nucleation.

$$A = \frac{z \cdot f_e^*}{v_w} \tag{77}$$

For HON,

$$A = \frac{z \cdot f_e^* \cdot A_p \cdot C_{par}}{a_w} \tag{78}$$

for HEN on nucleation-active microparticles without active centers on their equally sized surfaces of area A_p;

$$A = z \cdot f_e^* \cdot N_a \cdot C_{par} \tag{79}$$

for HEN on such particles each with the same number N_a of active centers on its surface

$$A = \frac{z \cdot f_e^*}{a_w} \tag{80}$$

for HEN on solid substrates or at the solution/gas interface in the absence of nucleation-active centers and

$$A = \frac{z \cdot f_e^* \cdot N_a}{A_s} \tag{81}$$

for HEN also on solid substrates or at the solution/gas interface, but with such centers on their surface. The factor A can be treated as $\Delta\mu$ independent when the super saturation is varied either in isothermal or isobaric regime, because the product zf_e^* changes relatively little in the pressure and temperature range typical for hydrate nucleation. In general, A has values much smaller for HEN than for HON [Kashchiev, 2000].

With an appropriate expression for the super saturation $\Delta\mu$ [Kashchiev & Firoozabadi, 2002a], Eq. (76) describes the rate of 3D one-component hydrate nucleation under various conditions. For nucleation in isothermal regime $\Delta\mu$ is determined by Eq. (71). Eq. (76) can then be given in the form

$$J = A \cdot S \cdot \exp\left(\frac{-B}{\ln^2 S} \right) \tag{82}$$

which represents only implicitly the dependence of *J* on the imposed pressure *P*. Here the practically *S*-independent kinetic parameter *A* is specified by Eqs. (77)– (81), and the dimensionless thermodynamic parameter *B* and the supersaturation ratio *S* are defined by

$$B = \frac{4 \cdot c^3 \cdot v_h^2 \cdot \sigma_{ef}^3}{27 \cdot (k \cdot T)^3} \tag{83}$$

$$S = \left(\frac{\varphi(P,T) \cdot P}{\varphi(P_e,T) \cdot P_e} \right) \cdot \exp\left(\frac{\Delta v_e \cdot (P - P_e)}{k \cdot T} \right) \tag{84}$$

Similarly, in isobaric regime $\Delta\mu$ is given by Eq. (72) and J from Eq. (76) can be expressed as the following explicit function of the undercooling ΔT :

$$J = A \cdot \exp\left(\frac{\Delta s_e \cdot \Delta T}{k \cdot T} \right) \cdot \exp\left(\frac{-B'}{T \cdot \Delta T^2} \right) \tag{85}$$

Here the kinetic parameter *A* is also given by Eqs. (77)–(81) and can be treated as ΔT independent, because hydrate nucleation in aqueous solutions occurs at relatively small undercoolings. The thermodynamic parameter B' (K^3) is defined by

$$B' = \frac{4 \cdot c^3 \cdot v_h^2 \cdot \sigma_{ef}^3}{27 \cdot k \cdot \Delta s_e^2} \tag{86}$$

and its value for a given hydrate, analogously to that of *B*, is again largely determined by σ_{ef}.

The kinetics of nucleation of one-component gas hydrates in aqueous solutions are analyzed. The size of the hydrate nucleus and the work for nucleus formation are determined as functions of the supersaturation $\Delta\mu$. Expressions for the stationary rate *J* of hydrate nucleation are derived. These expressions describe the *J* ($\Delta\mu$) dependence for homogeneous nucleation and for heterogeneous nucleation at the solution/gas interface or on solid substrates and nucleation-active micro-particles in the solution.

5. Determine the Hydrate Slurry Solid Mass Fractions

The amount of hydrates formed as a function of slurry volume was calculated using the mass flow meter slurry density measurement. The density of the three-phase mixture ($\rho_{Hyslurry}$) is given by:

$$\rho_{Hyslurry} = \frac{\rho_{CO_2Solution} \cdot \rho_{hydrate}}{\rho_{CO_2Solution} \cdot x_{CO_2hydrate} + \rho_{hydrate} \cdot (1 - x_{CO_2hydrate})} \tag{87}$$

The saturated CO_2 solution density model proposed by Duan *et al*. (2008) for liquid CO_2-H_2O mixtures was defined using the equation:

$$\rho_{CO_2Solution} = \frac{M_{CO_2Solution}}{V_{CO_2Solution}} \tag{88}$$

where

$$M_{CO_2Solution} = x_{CO_2} \cdot M_{CO_2} + x_{H_2O} \cdot M_{H_2O} \tag{89}$$

$$V_{CO_2Solution} = V_1(1 + (A_1 + A_2P)x_{CO_2}) \tag{90}$$

$$Ai = Ai_1T_2 + Ai_2T + Ai_3 + Ai_4T_{-1} + Ai_5T_{-2} \qquad (i=1,2) \tag{91}$$

The molar fraction of CO_2 in the solution is related to the solubility as shown:

$$x_{CO2} = \frac{\left(C_s / M_{CO_2}\right)}{\left(C_s / M_{CO_2}\right) + \left(1 / M_{CO_2}\right)} \tag{92}$$

and

$$x_{H_2O} = 1 - x_{CO_2} \tag{93}$$

where C_s is proposed by Duan *et al.* (2006). Teng *et al* 1996 proposed another similar equation to calculate CO_2 hydrate density:

$$\rho_{hydrate} = \frac{46 \cdot M_{CO_2}}{N_0 \cdot a^3} \cdot \left(0.409 + \frac{x_{CO_2}^{hydrate}}{1 - x_{CO_2}^{hydrate}}\right) \tag{94}$$

Where, 46 is the number of water molecules in a unit CO_2 hydrate cell, M_{CO2} =44 g/mol. It is found that density of CO_2 hydrate, $\rho_{hydrate}$, is influenced strongly by $x_{CO_2}^{hydrate}$. The relationship between the occupancy η and the molar fraction of CO_2 in the hydrate $x_{CO_2}^{hydrate}$ is derived as:

$$\eta = \frac{5.75 \cdot x_{CO_2}^{hydrate}}{1 - x_{CO_2}^{hydrate}} = \frac{8}{x + y} \tag{95}$$

where $x \leq 2$ and $y \leq 6$, represent the numbers of the occupied 5^{12} and $5^{12}6^2$ cavities. As CO_2 hydrate is a nonstoichiometric compound, therefore hydration number is variable.

It is seen in Table 2 if all the cavities in the hydrate are occupied (i.e. x=2; y=6; η = 100), n_w equals to 5.75; CO_2 hydrate has the maximum density value estimated from the perfect crystallographic. Teng et al (1996)'s prediction $\rho_{hydrate}$ = 1134kg/m^3 very good agreement with Uchida et al (1995), Takenouchi and Kennedy (1965). Their prediction is with ~2% deviation from Stackelberg and Müller (1954), ~2.7% deviation from Ota and Ferdows (2005)'s simulation. With different occupancies of cavities, the mole fraction of CO_2 in the CO_2

hydrate $x_{CO_2}^{hydrate}$, occupancy η as well as hydrate density will be different. With decreasing numbers of occupied cavities and the mole fraction of CO_2 in the CO_2 hydrate, CO_2 hydrate density decreases; with increasing hydration number, CO_2 hydrate density decreases. Usually, the hydration number is expressed within the range of $5.75 \leq n_w \leq 7.67$.

However, the following processes will decrease mole fraction of CO_2 in the CO_2 hydrate, increase hydration number to the value higher than 7.67, resulting in decreasing of density. i.e. Form hydrates in highly non-equilibrium conditions (CO_2 solution is not supersaturated); not enough CO_2 gas; fast crystallization; very much interstitial fluid comparing with CO_2 gas; small free gas volume in the reactor …etc; therefore, it is likely to have the cases where CO_2 hydrates are not easy to form (North *et al* 1998, Morgan *et al* 1999); form hydrates lighter than water and float observed by Unruh and Katz (1949) and North *et al.* (1993). With even lower value of mole fraction of CO_2 in the CO_2 hydrate, unstable paste-like CO_2 hydrate composite will be formed (Gborigi *et al* 2007);

Table 2. Summarized data from Teng *et al* 1996

x; y	x=2; y=6	x=1; y=6	x=0; y=6	x=0; y=5	x=0; y≤4
n_w	5.75	6.57	7.67	9.2	≥11.5
$x_{CO_2}^{hydrate}$	0.148	0.132	0.115	0.098	≤ 0.080
η (%)	100	83	75	62.5	≤ 50
$\rho_{hydrate}$	1134	1097	1049	1007	≤ 965

For Single Crystal Diffraction Studies by Udachin *et al* 2002, hydrate crystals of natural gas hydrates grew under essentially equilibrium pressure at 3 °C over a period of months to years in sealed Pyrex tubes containing ice and the guest components. Circone *et al* 2003 synthesized CO_2 hydrate from CO_2 liquid and H_2O solid and liquid reactants at pressures between 5 and 25 MPa and temperatures between 250 and 281 K. Based on above description of crystal process, we conclude that most of thermodynamic properties of CO_2 hydrate are obtained from stable hydrate crystal which is usually formed under conditions of small volume; less interstitial fluid; excess of CO_2 gas or CO_2 liquid; slow crystallization up to years; synthesis pressure was much higher than hydrate equilibrium pressure.

However, the CO_2 hydrate formed under arbitrary conditions may not be perfectly crystalline. Both the lattice measurements and the cage occupancy measurements may need revision. If only the large cavities are occupied (i.e. n_w =7.67), then $\rho_{hydrate}$ = 1049 kg/m^3 from Teng's prediction, which is only slightly different from the measured value $\rho_{hydrate}$ =1040 kg/m^3 (Uchita *et al*, 1995), with ~3.3% deviation from Ota and Ferdows (2005)'s simulation.

Circone et al 2003 suggested the composition of the hydrate should reflect the hydrate formation pressure P above three phase equilibrium (Lw-H-V) pressure Po, the ratio of P/Po should be a good relative indicator of sample composition for purpose of comparing samples prepared under different conditions. He also defined overpressure as the difference between the pressure of hydrate formation and the hydrate equilibrium pressure at the experimental

temperature. If the hydrate formation pressure equals to or lower than Po, hydrate formation will not succeed. For the protocol of CO_2 hydrate formation by controlled CO_2 gas injection, when the suitable hydrate formation temperature achieved, ratio of P/Po is larger than 1, overpressure is small, small portion of hydrates (e.g. ~10%) will begin to form. Most likely, the large cavities of hydrate are not fully occupied (see table 1, i.e. n_w =9.2), density of hydrate is about 1007 kg/m^3. This is due to low concentration of CO_2, fast crystallization and much the interstitial fluid initially. Accompanying the increase of P/Po ratio and overpressure due to gas injection, at constant temperature, most likely CO_2 gas occupied the large cavities of hydrate (i.e. n_w =7.67) and results in density about 1040 kg/ m^3. Thereafter, the overall hydrate density is less than 1040 kg/m^3. In our study, $\rho_{hydrate}$ =1036 kg/m^3 is referred.

6. Experimental Setup

6.1 The Pilot CO_2 Hydrate Slurry Test System

The new test rig is mainly equipped with the following components: a high-pressure pump, one double tube heat exchanger, two chillers, one consumer and CO_2 gas injection unit. See figure 6. The double tube heat changer is made of stainless steel. It consists of two separated parts.

Wherein the primary fluid is coolant while the secondary fluid is the test fluid. The length of heat exchanger is about 28 m, with height of 1.1 m. The outer diameter of the secondary fluid pipe is 33.5 mm and primary fluid pipe is 49 mm, see figure 7. The safety operation pressure of the system is 40 bar. All the experimental data are obtained by Agilent 34980A data acquisition system.

This pilot CO_2 hydrate slurry test system consists of three sub-circuits (See Fig.8). The primary circuit is for coolant (in colour blue). The secondary circuit is for the test fluid e.g. water, CO_2 solution, CO_2 hydrate slurry (in colour green). The third circuit is for CO_2 gas injection (in colour red). Table 3 lists the technical information of major components. The temperatures of the whole loop are monitored by Pt 100 at different locations. See Table 4 the list of temperature sensors.

Fig.6: The pilot CO_2 hydrate slurry test rig

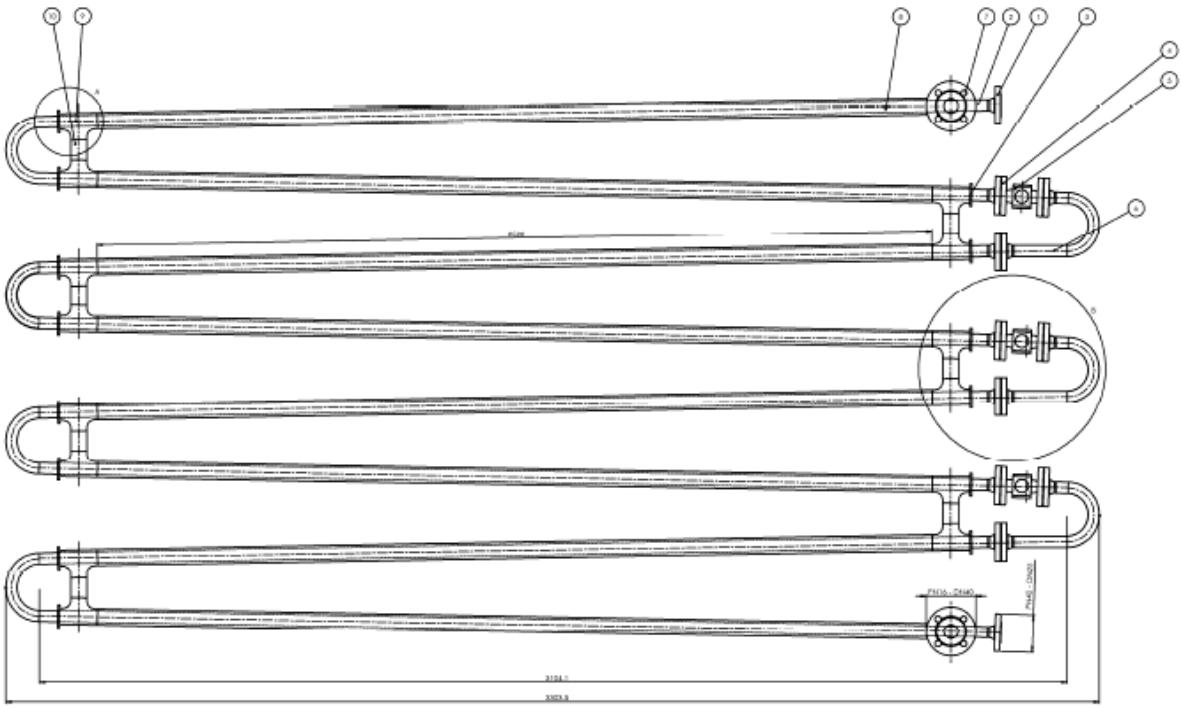

Fig. 7: Schematic drawing of double tube heat exchanger

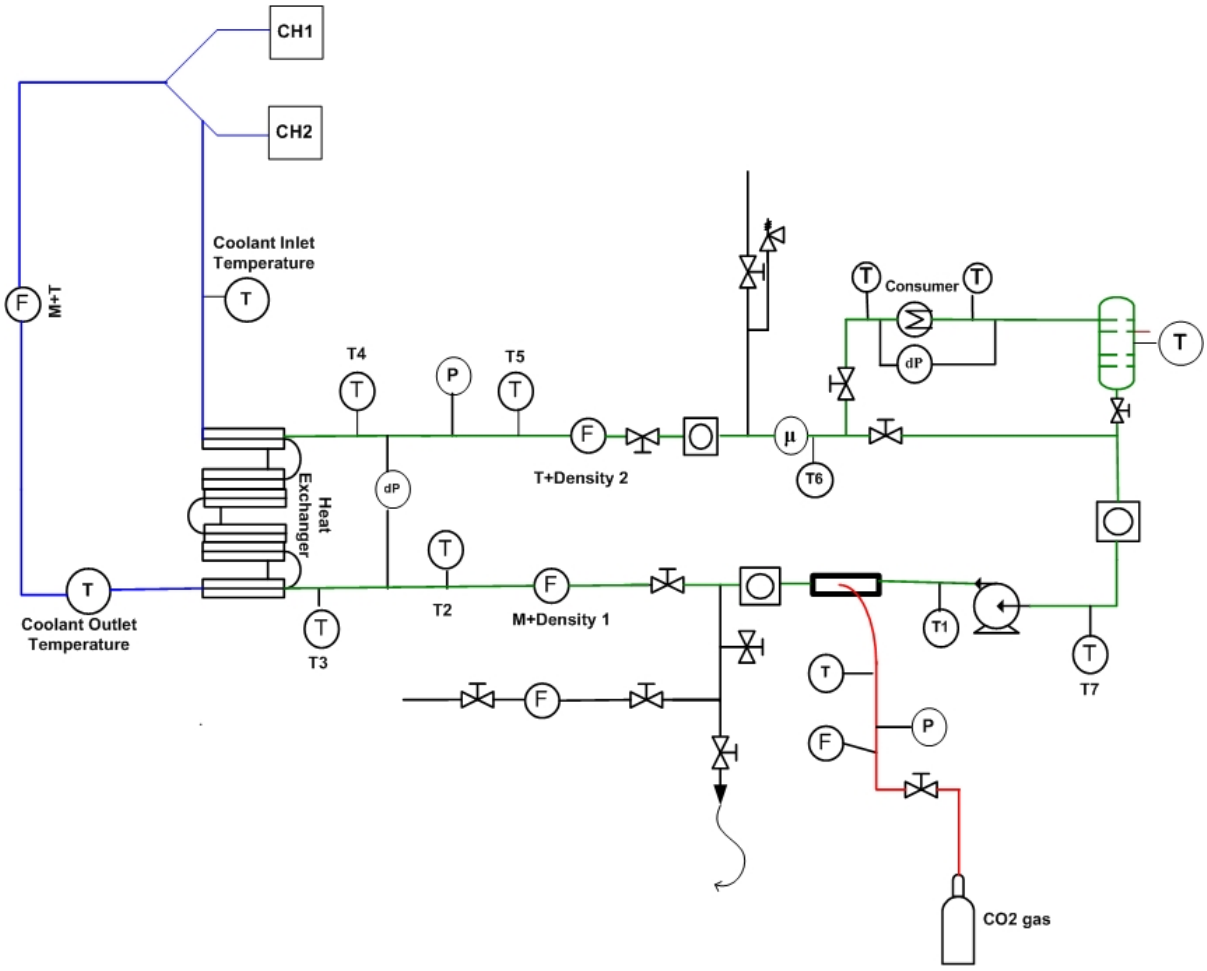

Fig. 8 Schematic drawing of the pilot CO_2 hydrate slurry test system

Table 3. Technical information of major components in the test rig

Symbol	Description	Manufacture	Model
	CO_2 gas	Carbagas	
	High pressure pump	Sterling	AEHA 1201 ABAF3 4B4
	Gas inject device	Tis	
	Double tube heat exchanger	Tis	
	High pressure consumer	Günter	S-GGHF040.1C/17-AW/20P
F	Mass flow meter	Endress+Hauser	Promass 83F25
F	Mass flow meter	Endress+Hauser	Promass 63F25
F	Mass flow meter	Endress+Hauser	Promass 63F40
F	Mass flow meter	Endress+Hauser	Promass 63AS02
P	Pressure transducer	Wika	Type S-10 0…40 bar G1/2B
P	Pressure transducer	Wika	Type S-10 0…100 bar G1/2B
μ	Viscometer	Hydramotion	XL7-100
ΔP	Differential pressure meter	Endress+Hauser	Deltabar S PMD/75
ΔP	Differential pressure meter	Endress+Hauser	PMD235-KBBH1EA1C
T_1-T_7	Temperature Sensor	Alphatemp Technology	Pt 100
T	Thermocouple	Thermocoax	K-type
	Storage tank	Tis	
CH1	Chiller	Huber	IC 060W-H8
CH2	Chiller	Huber	UC 055 Tw
	Observation window	Axima	
	Safety valve	Seetru	CF 3M 40bar

Table 4. Nomenclature for the temperature measurement

Component	Description
T	Temperature of injected CO_2 gas
T_1	Temperature of the fluid after the pump
T_2	Temperature of the fluid prior to reach the entrance of heat exchanger
T_3	Temperature of the fluid at the entrance of heat exchanger
T_4	Temperature of the fluid at the exit of heat exchanger
T_5	Temperature of the fluid after the exit of heat exchanger
T_6	Temperature close to viscometer
T_7	Temperature of the fluid before the pump
Coolant Inlet Temp	Temperature of coolant at the entrance of primary circuit
Coolant Outlet Temp	Temperature of coolant at the exit of primary circuit

6.1.1 Primary Circuit

There are two chillers denoted as CH1 and CH2 employed in the primary circuit and displayed in Fig. 8 .The primary circuit uses Neutragel/Water 33 % mixture as coolant to cool down (or heat up) the double tube heat exchanger; technical data of chillers are shown by Table 5. The coolant circuit is monitored by one mass flow meter and two PT100 sensors, named coolant inlet temperature and coolant outlet temperature respectively. The specific heat capacity of Neutragel/Water 33 % mixture was measure by Micro DSCVII Calorimeter. Results are shown in figure 9.

Table 5. Technical data of Chillers

Temperature (°C)	UC055Tw-3	IC 060w-H8
	Cooling Power (kW)	
15	5.5	6
0	4	6
-10	2	3.8

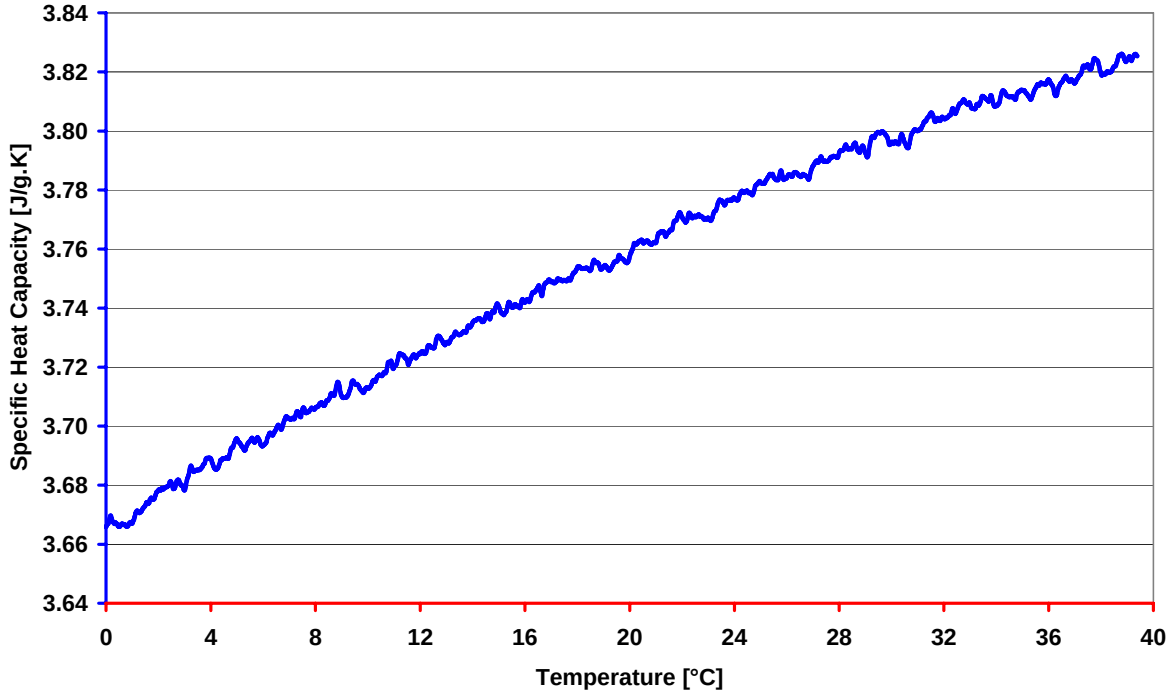

Fig. 9: Specific heat capacity of Neutragel/Water 33 % mixture as function of temperature

6.1.2 Secondary Circuit

To simplify the CO_2 hydrate slurry production system, double heat exchanger will be used to produce the hydrate slurry directly and continuously. The double tube heat exchanger is the core part of secondary circuit. Flow of the fluids in the secondary circuit is driven by high pressure pump; one pressure transducer is for the fluid pressure; the densities as well as mass flow rates of the fluids in the secondary circuit are monitored by two mass flow meter respectively; one differential pressure flow meter is to measure pressure drop on the double tube heat exchanger; hydrate dissociation process is conducted in the higher pressure consumer. The pressure drop on the consumer is measured by another differential pressure flow meter; temperatures of the fluids at different locations are recorded by 7 Pt100 probes, namely $T_1 \ldots T_7$ (see Table 4); 3 small visualisation windows on the double tube heat exchanger; another 3 big visualisation windows locate separately between the pipes of the secondary circuit. Hydrates formation and dissociation can be observed clearly through these six windows.

6.1.3 CO_2 gas Circuit

One CO_2 bottle feeds the gas circuit to the one single injection point of the CO_2 hydrate slurry loop. Gas temperature is monitored by one K-type thermocouple (T), pressure is recorded by pressure transducer and mass flow rate is recorded by mass flow meter.

6.2 Measurement Techniques

6.2.1 Measurement of Temperature

A new temperature sensor was developed by Alphatemp Technology, Ltd in UK. The objective is to obtain a high precision temperature measurement in a point. The effective sensor part diameter is 1.2×10 mm (See Fig.10).

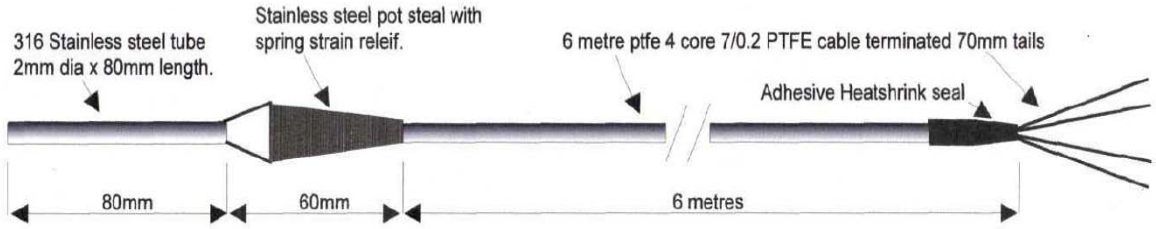

Fig.10: Schematic drawing of temperature Sensor PT100

All the temperature probes were calibrated before the experiments. Three different temperatures -5°C, 0°C and 5°C were tested to calibrate all the temperature sensors respectively in Huber Ministat Refrigerated Circulating Bath together with two reference probes. Two reference probes were calibrated annually in an appointed company. The maximum temperature deviation between the reference probe and temperature sensor was about ± 0.2 %. After the calibration, temperature sensors are within an accuracy of ± 0.04 °C. They monitor temperature from T_1 to T_7 and primary circuit at different locations in the rig.

6.2.2 Measurement of Mass Flow Rate and the Fluid density

Mass flow rate of all working fluids in the experimental rig were measured by Endress+Hauser mass flow meters, see Fig.11. Densities of water, CO_2 solution as well as CO2 hydrate slurry are also measured by such mass flow meters, which were calibrated according to the suitable temperature and pressure range for hydrate formation and dissociation. The maximum deviation of mass flow rate was about ± 0.01kg/s and maximum deviation of density was about ± 0.4 kg/m^3.

6.2.3 Measurement of the Heat Capacity and Enthalpy

Heat capacity and enthalpy are determinated by a digital scanning calorimetry (DSC). The base calorimeter was selected to be easily adapted and modified to meet the whole specifications previously described: Micro DSCVII by Setaram. The calorimetric furnace is made of a double aluminium wall, see Fig.12. The experimental and reference vessels are inserted into the furnace by two cylindrical cavities. The main advantage relates to the system of cooling, which is provided by Peltier effect. This system avoids the handling of refrigerating fluids such as liquid nitrogen. The minimum temperature that can be reached is about –45 °C and the maximum temperature is 120 °C.

Fig.11: Endress+Hauser Mass flow meter to measure mass flow rate and density

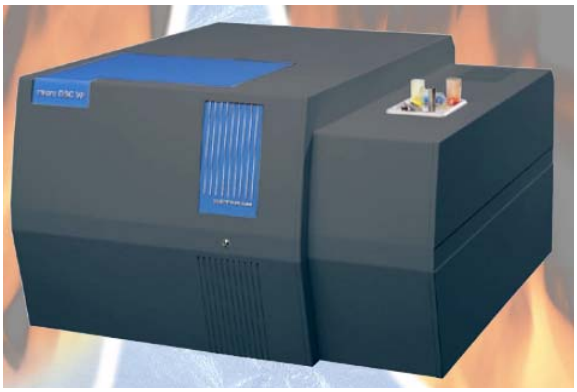

Fig. 12: SETARAM Micro DSCVII Calorimeter

6.2.4 Measurement of the Viscosity

Viscosity is a shear measurement and can only be truly assessed under shear conditions, so it was decided to use shear waves. The XL7-100 on-line viscometer was selected and be used to measure viscosity in our experiments. The XL7-100 viscometer produced by Hydramotion Ltd. is in a class of instruments called vibrational or resonant viscometers. Vibrational viscometers work by creating waves. The solid stainless steel sensor element of XL7-100 is submerged in the fluid and made to move back and forth microscopically at a high frequency. This is called "resonance". As the surface of the sensor shears through the liquid, energy is lost to the fluid because of its viscosity. The dissipated energy is accurately measured by microprocessor-controlled electronics and then equated back to viscosity. Higher viscosity causes a greater loss of energy and hence a higher reading.

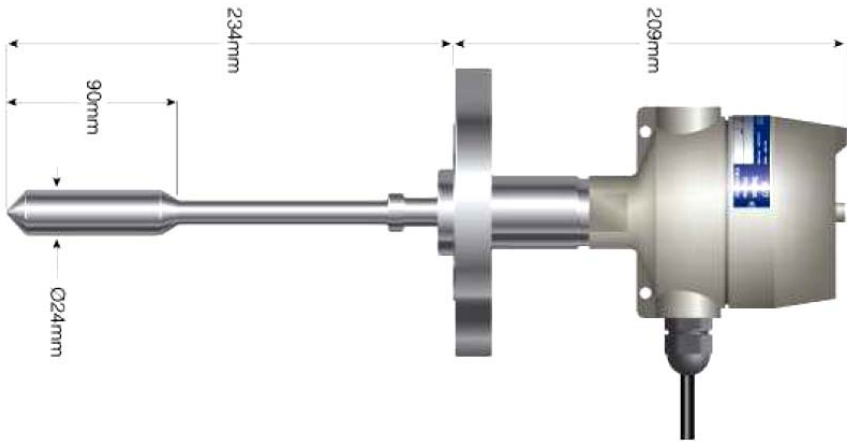

Fig. 13: XL7-100 Process Viscometer in the Experimental Loop

6.3 Water Test

Prior to examine CO_2 hydrate slurry, water test was performed on the system. Water was cooled down by chillers. The setting temperature for the chillers was 1°C. During the cooling process, temperature, density, viscosity, pressure drop and mass flow rate were recorded.

6.3.1 Water Density

Online density measurements of tab water were performed by mass flow meter under atmosphere and dynamic conditions in the temperature range of 1-30°C. Results were compared with the predicted values obtained from the water EoS proposed by Wagner and Pruss (2002). The experimental values are in a good agreement with the literature data with a maximal deviation of 0.07 % found at lower temperatures.

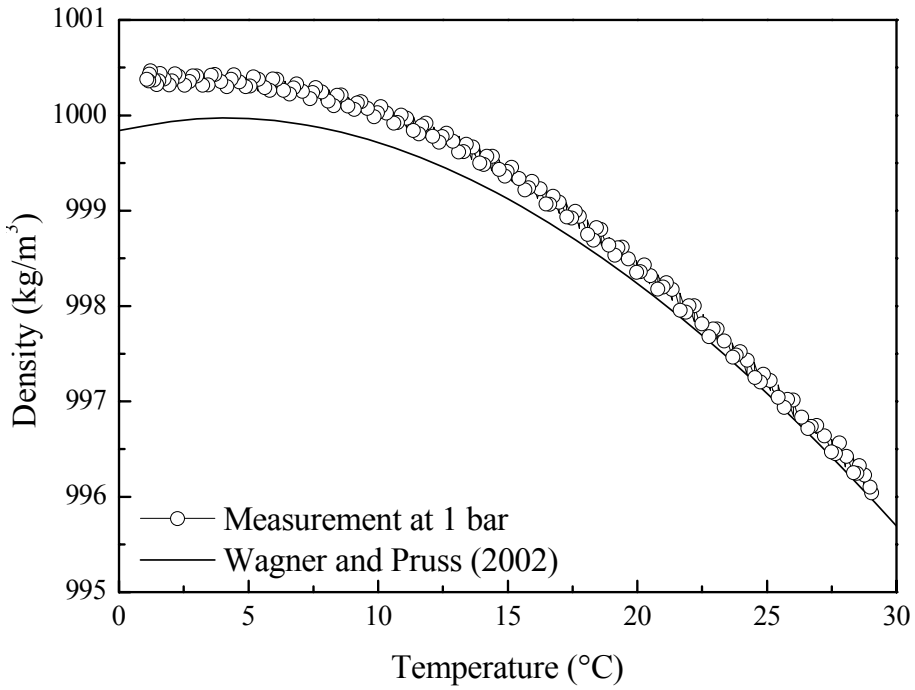

Fig.14: Comparison between measurements and model predicted results of density of tab water

6.3.2 Dynamic Viscosity

Online measurements of the viscosity of tab water under atmospheric and dynamic conditions were conducted to evaluate the "resonance" method of the XL7-100 viscometer. The experimental values are in good agreement with the viscosity equation proposed by Watson *et al.* (1980) and the absolute deviation is within 1 %. The "resonance" method can be applied to determine the viscosity of the fluid online with a maximum uncertainty of 1 %, see figure 15.

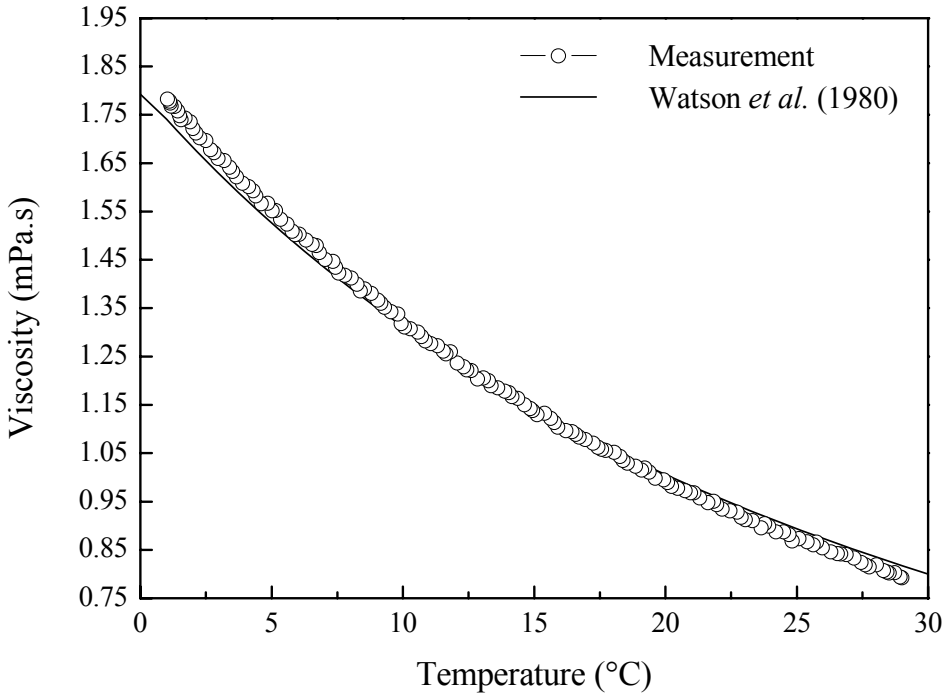

Fig. 15: Comparisons between Measurements and Model Results of Viscosity of Ordinary Water

6.3.3 Pressure Drop

Fig. 16 shows the measurement of pressure drops on water side of the double tube heat exchanger as a function of mean velocity of the water in pipeline. The pipeline length between the negative and positive side of the differential pressure transmitter is 28.9m. Prior to the test, the process of "Position zero adjustment" is done to the differential pressure transmitter as a calibration procedure. The employed test water temperature was between 8-10°C, density was about 1000.26 kg/m^3. As the lowest mean velocity (v=0.5m/s) corresponding to the Reynolds number is as large as 12674, which means the flows are all turbulent flows at all velocity in pipeline of the secondary circuit. Between water velocities of 0.5-1.5m/s, the pressure drops were measured. As it is seen, the pressure drops increase with the increasing of mean velocity.

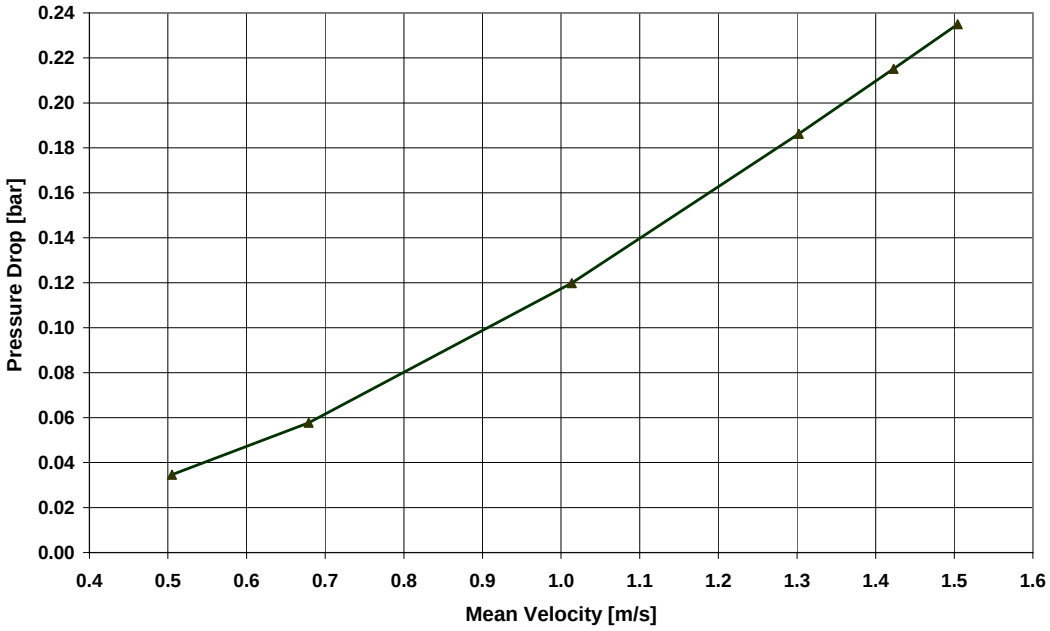

Fig.16: Pressure drops on heat exchanger as a function of mean velocity of the water

6.3.4 Energy Balance

The measurement of single phase fluid water was first conducted to confirm the reliability of the heat transfer test system. The energy balance between the Coolant (Neutragel/Water 30% mixture) side and water side on double tube heat exchanger are realized at steady state of system running. At steady state, it can also be assumed that: the specific heat capacity (Cp) hot and (Cp) cold are constant; heat loss to the surroundings is negligible and fluid flow is steady state and parallel.

$$\dot{Q} = \dot{m}_h \cdot c_{p_h} \cdot (T_{hi} - T_{ho}) = \dot{m}_c \cdot c_{p_c} \cdot (T_{co} - T_{ci}) \tag{96}$$

Table6. Flow Properties of water and coolant

Fluid	Specific Heat (J/kg.K)	Density (kg/m^3)	$\dot{m}$ (kg/s)	ΔT (°C)	$\dot{Q}$ (W)
Coolant	3670	1047	1.02	1.6	5989
Water	4196	1000.1	0.60	2.31	5816

It can be seen from Table 6 the heat transferred between coolant and water is well balanced in water test and heat loss is within 3 %.

6.3.5 Calculations of Heat Transfer Coefficient

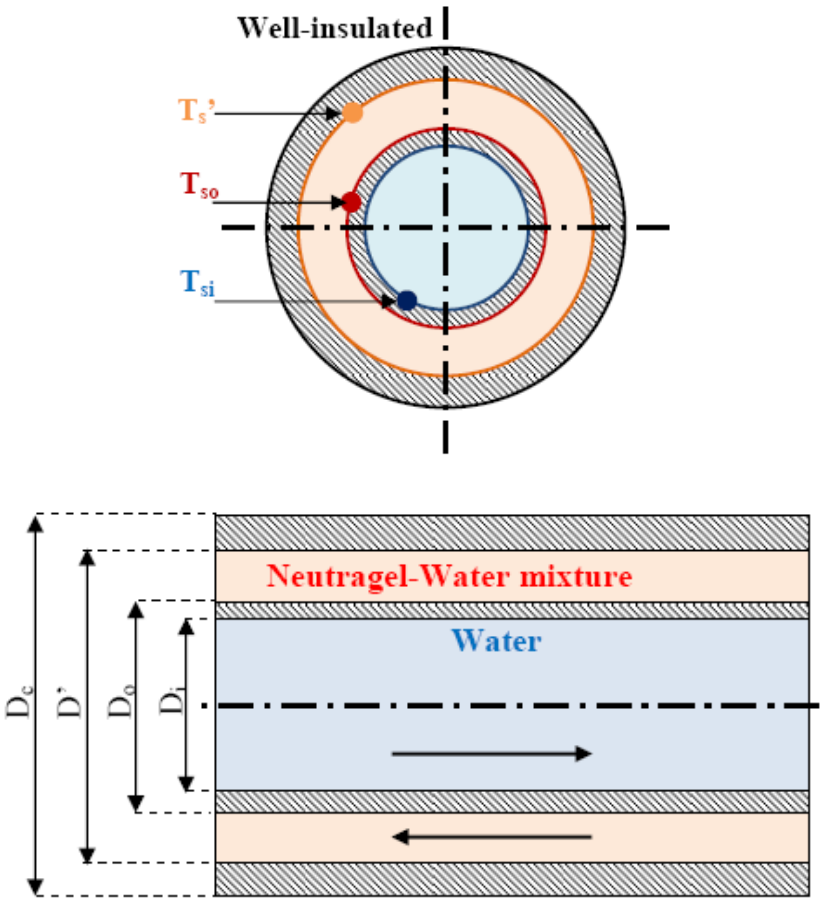

Fig.17: Cross-section of pipes of double-tube heat exchanger

Table7. Hydraulic diameter for water and coolant

Water	Coolant
$D_h = D_i$	$D_h = 1.06 \times 10^{-2}\,m$
$D_h = 2.97 \times 10^{-2}\,m$	$D_h = D' - D_o$

D_i=0.0297m, D_o=0.0337m. D'=0.0443m, D_c=0.0483m. L=22.04m. A=2.333 m^2.

Table8. Heat transfer coefficients and overall heat transfer coefficient

Parameters	**Water**	**Coolant**
$\dot{m}$ (kg/s)	0.6	1.02
Re_{Dh}	$Re_{Dh} = \frac{4 \cdot \dot{m}_i}{\mu_i \cdot \pi \cdot D_i}$	$Re_{Dh} = \frac{4 \cdot \dot{m}_o}{\mu_o \cdot \pi \cdot (D'+D_o)}$
	$Re_{Dh} = 19431$ turbulent flow	$Re_{Dh} = 4690$ turbulent flow
μ (Pa/s)	0.001332	0.003556
λ (W/m.K)	0.579	0.479
Pr	$Pr = \frac{\mu . c_p}{\lambda}$ $Pr = 9.6$	$Pr = \frac{\mu . c_p}{\lambda}$ $Pr = 27.5$
Nu_{Dh}	$Nu_{Dh} = \frac{h \cdot D_h}{\lambda}$ $Nu_{Dh} = 122.4$ $Nu_{Dh} = 0.023\, Re_{Dh}^{\frac{4}{5}}\, Pr^{0.3}$	$Nu_{Dh} = \frac{\left(\frac{f}{8}\right)(Re_{Dh} - 1000)\, Pr}{1 + 12.7\left(\frac{f}{8}\right)^{\frac{1}{2}}(Pr^{\frac{2}{3}} - 1)}$ $f = \left[0.79 \ln(Re_{Dh}) - 1.64\right]^{-2}$ N_{Dh}=60.7 f=0.0394
h (W/m^2.K)	$h = 2386.3$	h = 2744.6
R	$R = \frac{T_{hi} - T_{ho}}{T_{co} - T_{ci}}$ R=1.4484	
P'	$P' = \frac{T_{co} - T_{ci}}{T_{hi} - T_{ci}}$ P'=0.3632	
P'R	$P' \cdot R = \frac{T_{hi} - T_{ho}}{T_{hi} - T_{ci}}$ $P' \cdot R = 0.5261$	
U (W/m^2.K)	$U = \frac{\dot{Q}}{A \cdot \Delta T_{LM}} = \frac{\dot{m}_h \cdot c_{p_h} \cdot (T_{hi} - T_{ho})}{(T_{hi} - T_{ci}) \cdot \frac{P' \cdot (R-1)}{\ln\left[\frac{1-P'}{1-P' \cdot R}\right]}} \cdot \frac{1}{\pi \cdot D_o \cdot L}$, U=1035 W/m^{2}K	

Based on log mean temperature difference approach and energy balance, the overall heat transfer coefficient of double tube heat exchanger for water is 1035 W/m^2.K. Heat transfer coefficient of water is 2386 W/m^2.K and heat transfer coefficient of coolant 2745 W/m^2.K. We can see heat transfer coefficients are very close each other between water and coolant.

7. Experimental Results and Discussion

7.1 CO_2 Solubility in Water

In general, solubility of CO_2, in the range of temperatures studied, decreases with increasing temperature at constant pressure. At constant temperature, solubility of CO_2 is found to increase with pressure, see Figure 18.

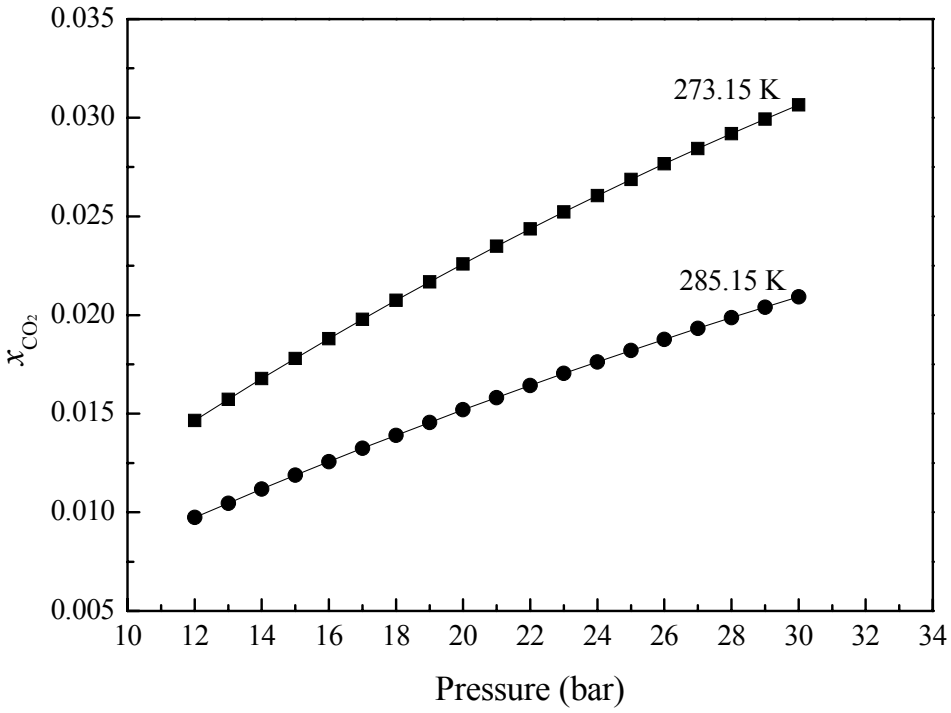

Fig.18: Solubility of CO_2 as a Function of Pressure and Temperature

7.2 Density Measurements of CO_2 Solution

The density change of the aqueous CO_2 solution as function of pressure and temperature was measured twice, denoted as measurements in two different groups. The ratio of CO_2 solution density to that of pure water under same conditions was plotted, see figure 18. The maximum deviation (MD) is 0.65% between measured and predicted values by Duan *et al*'s model (2006, 2008). As Duan's model is based on the equilibrium conditions and suitable for prediction of saturated CO_2 solution density, while under our experimental conditions, CO_2 solution is not very well saturated resulting in lower density comparing with predicted ones under same conditions.

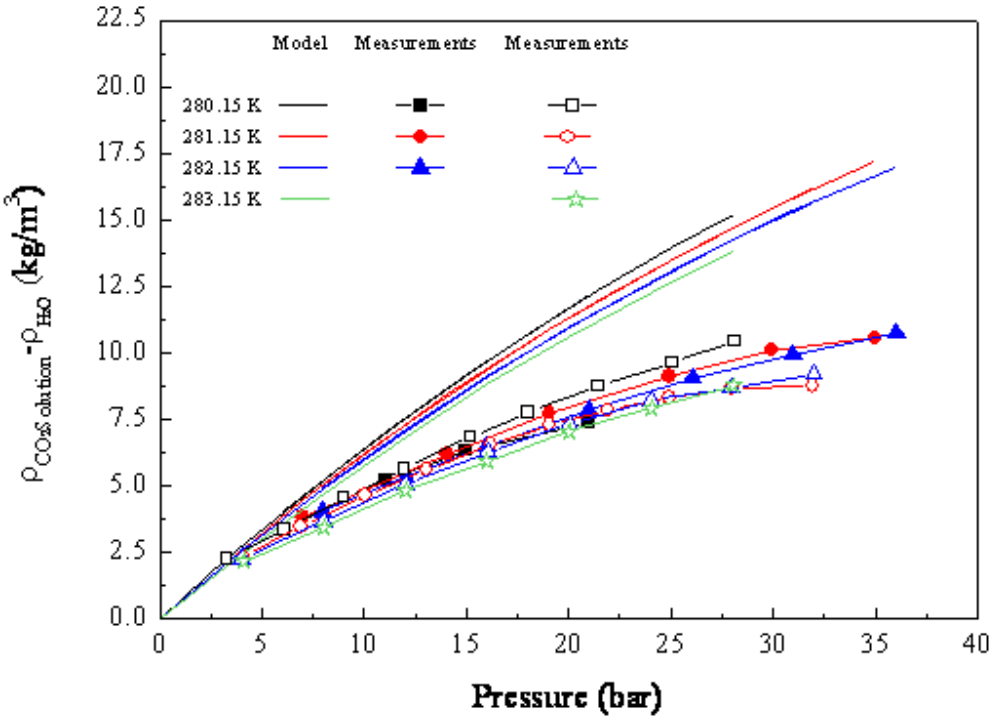

Fig.19: Comparisons of density differences between CO_2 solution and water under the same conditions

7.3 Formation of CO_2 hydrate Slurry by Super Cooling of Saturated CO_2 Solution

The water in the experimental loop was first cooled down to 9°C from ambient temperature simultaneously by chillers. Such fluid temperature is set above the hydrate formation temperature at given pressure to the loop to guarantee no hydrates formation when injecting CO_2 gas to the loop. Afterwards, about 2.4 kg of CO_2 gas was injected into the water in several times to form a CO_2 solution. Thereafter, CO_2 solution was undergoing super cooling by heat exchangers to 1°C. Hydrate formation was observed using a CCD camera with speed of 8000 frames/s.

It was observed during the experiments when suitable conditions for hydrate formation reached, small and few hydrate particles began to appear in 0.05s shown in Fig.20b. The appearance of the grey turbidity showed in Fig.20c was quite sudden and less than 0.5s. It is identified by a sudden change from a transparent CO_2 solution Fig.20a to a translucent one. Although the size if a critical hydrate nucleus is smaller than the particle size visible to the naked eyes, their number is sufficiently large to make the solution appear turbid. The hydrate particles have the same velocity as the liquid because the density of hydrate is very close to the density of CO_2 solution at the beginning.

Thereafter, huge amount of tiny hydrate particles formed like clouds, see figure 20d. Such hydrate particles began to grow into small hydrate crystals; solid mass fraction becomes larger and larger. The hydrate formation process lasted about 1.5s. Our experimental

confirmed the conclusion which has been reported by Aya et al. (1993). In their study, the hydrate formation time was found to be less than one second at 2-3°C and to increase to several seconds at 10°C.

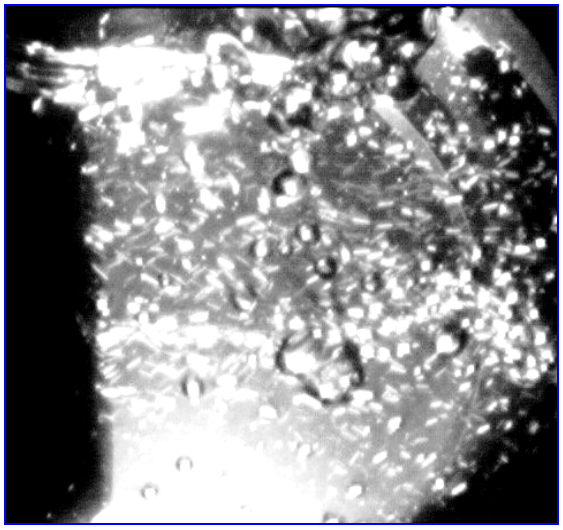

Fig.20a: The transparent CO_2 solution with a lot of CO_2 gas bubbles

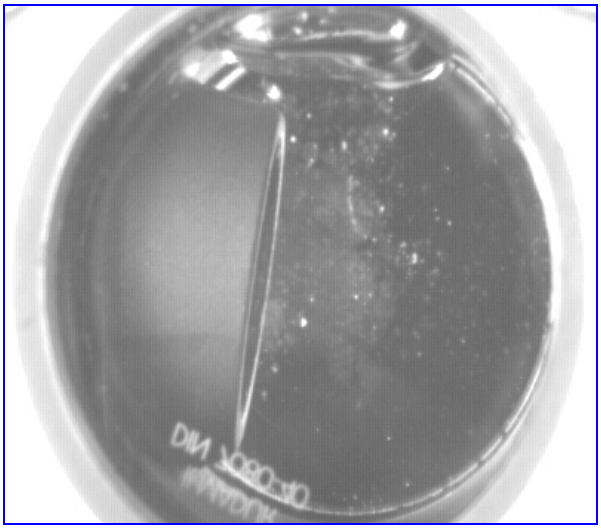

Fig.20b: First appearance of few CO_2 hydrate particles at the very beginning of formation

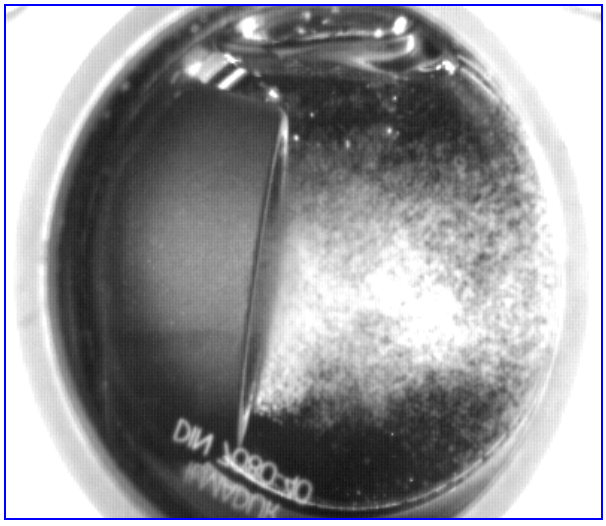

Fig. 20c: the sudden formation of grey turbidity indicating the beginning of the formation of CO_2 hydrates

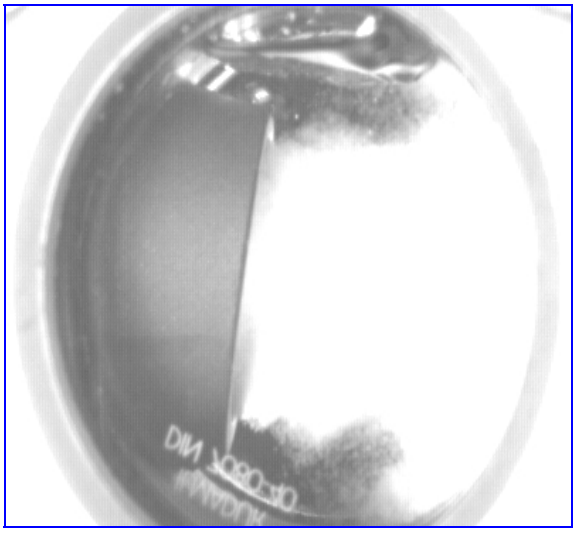

Fig. 20d: Huge amounts of white tiny hydrate formed like clouds

Fig.21 shows the physical appearance of large amounts of white hydrate formed and sinks. As CO_2 hydrates formation process takes only few seconds from supersaturated CO_2 solution

above 0°C, this means an efficient energy-saving is available considering CO_2 hydrate slurry as a kind of refrigerants.

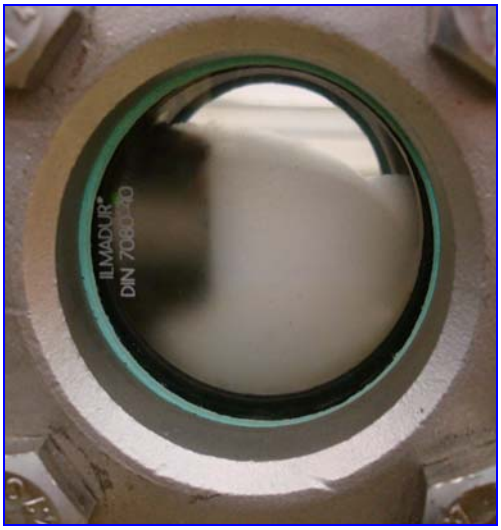

Fig.21: Agglomeration of white hydrates sink in the CO_2 solution

7.4 Apparent Viscosity

Only few works Oyama et al. (2003) and Uchida et al. (2003) have studied viscosity of the CO_2 solution at our range of pressure and temperature conditions, In general, viscosity of the CO_2 solution is found to increase significantly prior to hydrate formation. Measurements of the viscosity of the CO_2 solution was also found to increase with increasing pressure and solution density at a constant temperature see figure 22. We also found at constant pressure, viscosity of the CO_2 solution increases with decreasing of temperature. This indicates that high pressures and low temperatures aid more CO_2 gas to be dissolved into water, resulting in a higher viscosity of the solution. In other words, the viscosity of the CO_2 solution depends on the CO_2 solubility.

As many authors (Sloan, E.D., 1991; Fleyfel et al., 1994; Bishnoi and Natarajan 1996; Aya et al., 1997; Zhong and Rogers, 2000; Holder et al., 2001; Li et al 2008) reported that the temperature increased and the pressure decreased sharply at constant volume, which indicated the formation of hydrates. This is also being observed by us see figure 23. Fig.23 clearly shows at this transition zone coloured green, temperature suddenly decreased as well as pressure, while the density of the fluid abruptly increased indicating CO_2 solution has transformed into CO_2 hydrate slurry. Up to now, not so much information is available regarding the viscosity of CO_2 hydrate formation. In CO_2 hydrate formation process, Oyama et al. (2003) used a strain gauge viscometer to measure the viscosity deviation. Their measurements show that viscosity increases during the induction period. When the nucleation begins, the viscosity begins to decrease.

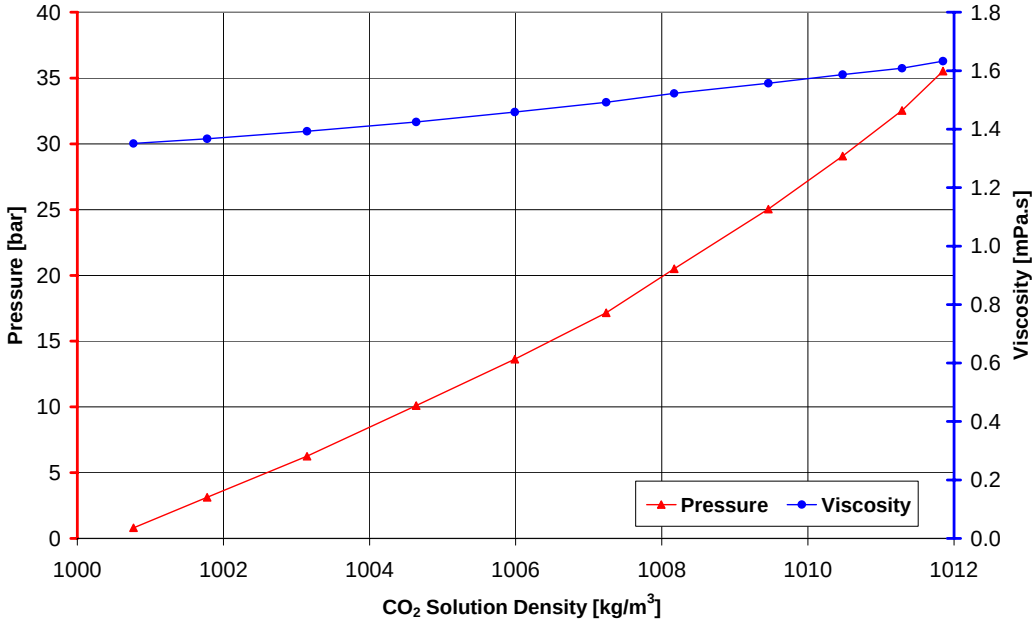

Fig.22: Pressure and temperature dependence of the CO_2 solution viscosity

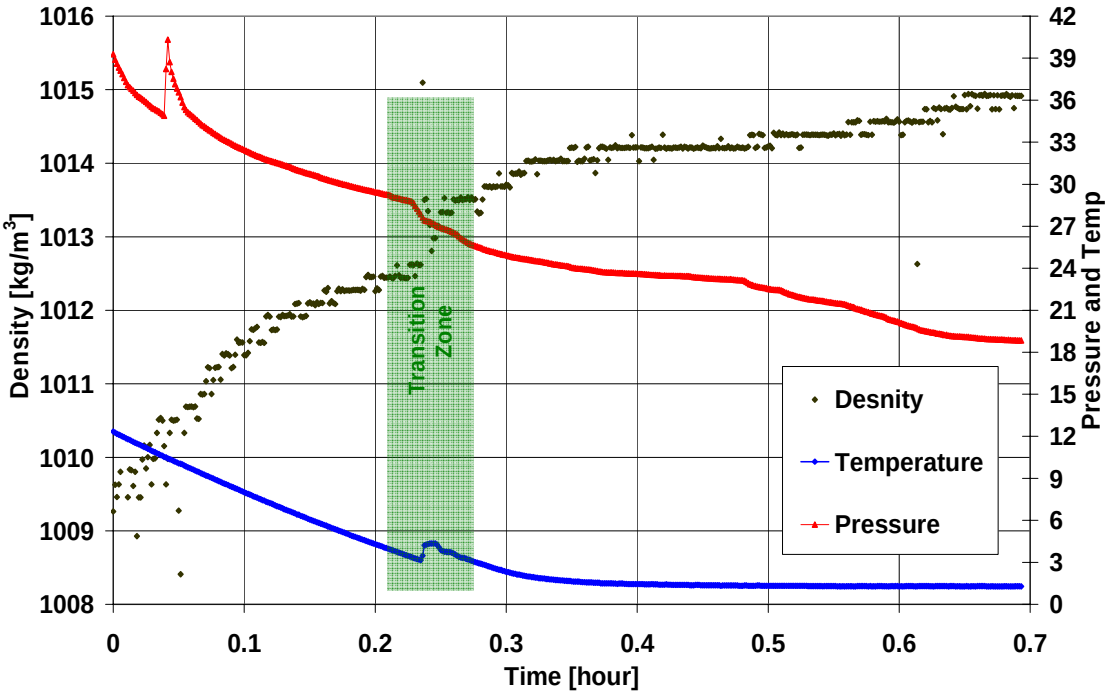

Fig. 23: Density, temperature and pressure evolutions during process of cooling saturated CO_2 solution to form CO_2 hydrate slurry

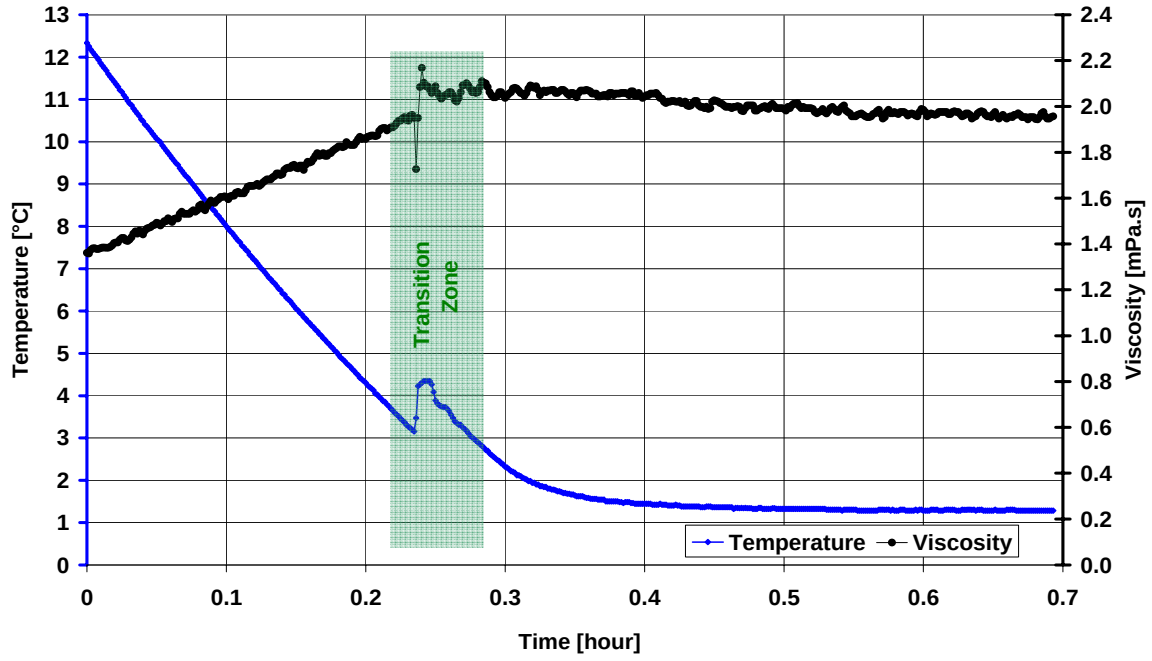

Fig.24: The evolutions of apparent dynamic viscosity of CO_2 solution transformed into CO_2 hydrate slurry vs temperature

Thus, the hydrate nucleation process is related to viscosity change before and after nucleation. They argue that the large number of water molecules tends to construct precursor hydrogen-bonded structures in the CO_2 solution leading to an increase in the viscosity prior to the hydrate formation. After nucleation and growth of the hydrate crystals, the amount of ordered water clusters should decrease.

Fig.24 reveals when the fluid temperature decreased, the CO_2 solubility increased which resulted in an increase in viscosity of the solution. When CO_2 solution reached the transition zone (in green), the CO_2 solution became supersaturated and CO_2 hydrates began to form immediately in the solution. As the formation of hydrates is an exothermic process, a large amount of heat was released to the sealed loop in a very short time. Consequently, external chillers were not able to respond fast enough to such sudden chemical reaction and temperature of the fluid from 3°C jumped to 4.4 °C in less than 15s. Because of this sudden increase of temperature, viscosity of the fluid decreased abruptly in 10s from 1.95 mPa.s to 1.73 mPa.s. However, 1.73mPa.s only being held in 7s and jumped to 2.17 mPa.s due to the nucleation of numerous CO_2 hydrate particles begins. Very soon after, apparent viscosity of CO_2 hydrate slurry began to decrease slightly accompanying the increase of slurry density. We argue this is probably the growth of the hydrate crystals continuously consumed the dissolved CO_2 in the solution resulting in the gradual increase of slurry density and loss of supersaturation in the solution, see density change in figure 23. The loss of supersaturation in the solution likely makes the viscosity decreases slowly. Due to the large heat capacity of water in this systems and continuous cooling of chillers, heat of hydrate formation can efficiently dissipate in the water phase, fluid temperature began to drops down fast again.

When the fluid temperature reached plateau, growth of the hydrate crystals gradually stopped and the slurry viscosity value was very closed to the final viscosity value of CO_2 solution prior to nucleation begins. We argue in the induction period and the beginning of hydrate nucleation, solution viscosity will increase while the growth of the hydrate crystals will slightly decrease the apparent viscosity. This finding differs from the measurements conducted by Oyama et al. (2003). This is probably due to different experimental conditions and scale.

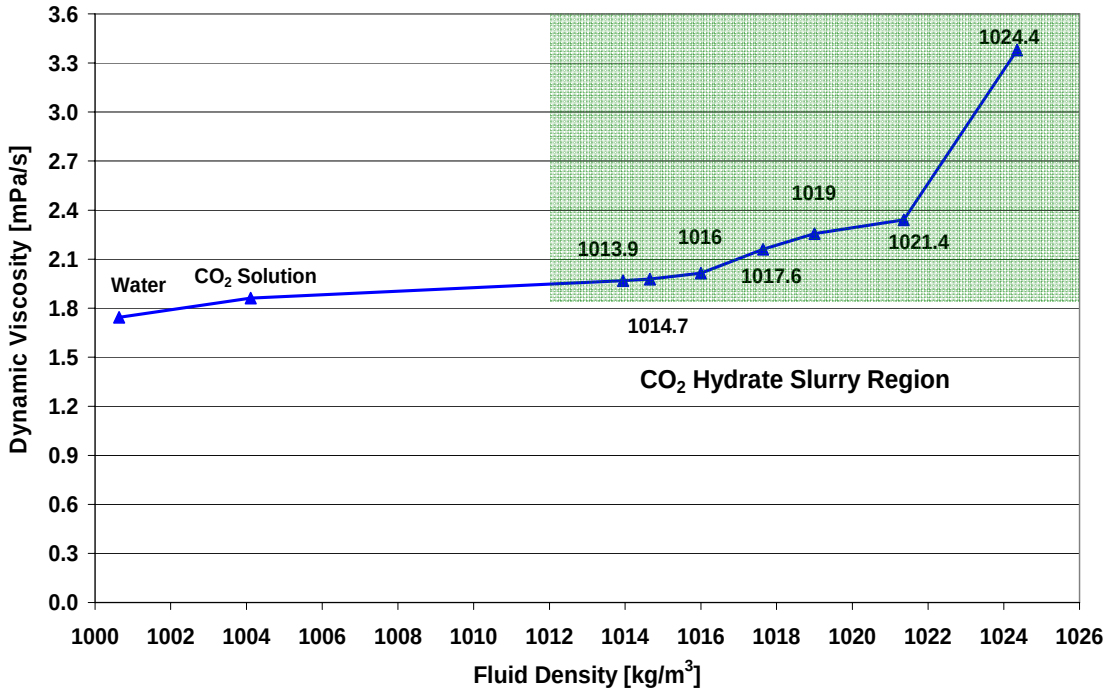

Fig.25: Apparent viscosity of CO_2 hydrate slurry as function of slurry density

Figure 25 reveals apparent viscosity of CO_2 hydrate slurry as function of slurry density. CO_2 hydrate slurry at different density was obtained by controlled CO_2 gas injection protocol under same experimental conditions. It is easy to be seen that CO_2 solution has higher viscosity value than that of water due to dissolved CO_2 gas. Viscosity of CO2 hydrate slurry with low density value (low solid mass fraction, e.g. 1013.9 kg/m3and 1014.7 kg/m3) is only little bit higher than that of saturated CO_2 solution. With increasing of hydrate slurry density (solid mass fraction), slurry viscosity also increases. A sharp increase of viscosity was found when density of hydrate slurry increases from 1021.4 kg/m3 to 1024.4 kg/m3 which corresponds mass solid fraction of 34 % and 45 % respectively. Even though the solid mass fraction is over 40%, viscosity of CO_2 hydrate slurry 3.4 mPa.s is much lower than that of ice slurry with same solid fraction resulting in excellent pump ability characteristics regarding power consumption even for a very high energy density.

7.5 Hydrate Formation and Dissociation Cycle

The water in the experimental loop was cooler down to 8°C simultaneously by two chillers °C. Such fluid temperature is set above the hydrate formation temperature at given pressure to

the loop to guarantee no hydrates formation when injecting CO_2 gas to the loop. Afterwards, 1.9124 kg CO_2 gas was injected into the water in several times to form a CO_2 solution. The final pressure of loop was about 40 bar. Thereafter, CO_2 solution was undergoing super cooling by heat exchangers. The temperature setting for the two chillers was kept at 1 °C during the cooling process. Hydrate formation was observed using a CCD camera and a transparent high-pressure observation window under dynamic conditions. When the hydrate slurry reached steady state, cooling was stooped and it was undergoing the dissociation process by heating up the fluid. When all the hydrates disappeared, CO_2 solution was cooled down again to reform the hydrate slurry. Such cycle was repeated 3 times.

Fig. 26 reveals the temperature and pressure cycles of hydrate formation and dissociation. As formation of hydrates by cooling consumes a lot of dissolved CO_2 gas, loop pressure decreases accompanying hydrate formation and increases accompanying hydrate dissociation. Fig. 27 reveals the pressure and density cycles of hydrate formation and dissociation. Formation of hydrates increases the bulk density while dissociation process decreases the bulk density. The first cycle has the highest density. Due to the escaped CO_2 gas from CO_2 solution to the space of the pipe during the dissociation process was unable to fully re-dissolve into CO_2 solution for the reformation hydrate process during the next cooling process, density of hydrate slurry will slightly decrease for each cycle. The solid fraction of hydrate for the experiments was about 17 %.

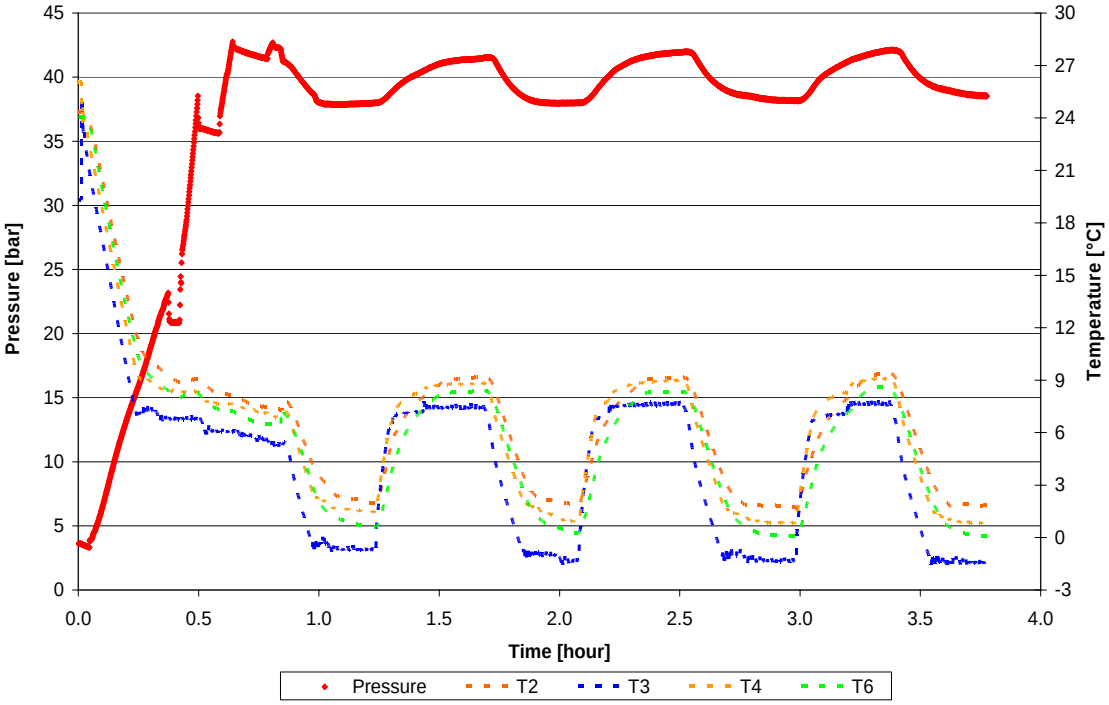

Fig.26: Pressure and temperature profiles of CO_2 hydrate slurry cycle

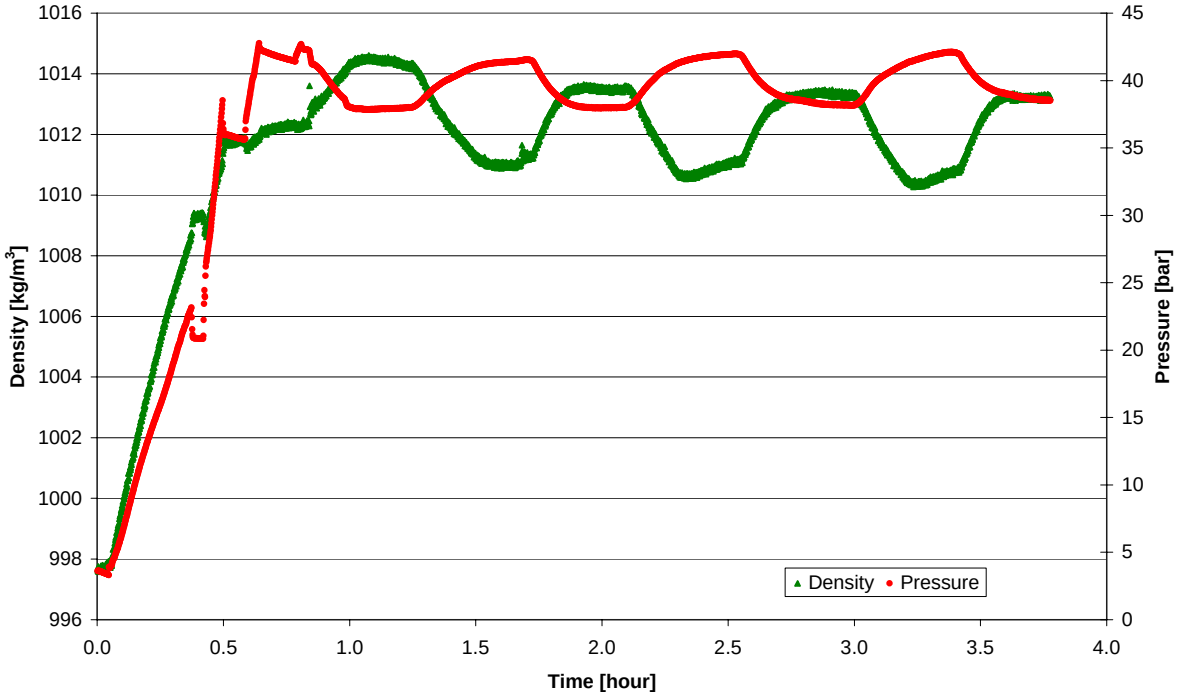

Fig.27: Pressure and density profiles of CO_2 hydrate slurry cycle

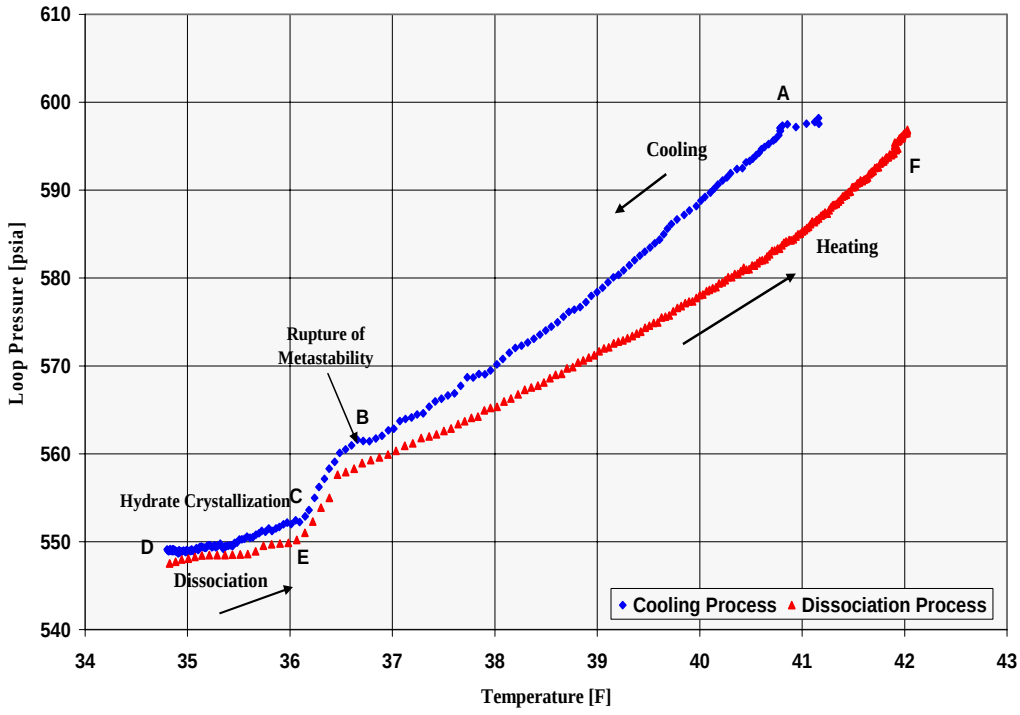

Fig.28: A complete temperature vs pressure cycle of CO_2 hydrate slurry formation by cooling after pressurization and dissociation

From figure 28 we can see that the experiments started at point A where the loop pressurization process was over. A-B is the cooling curve which indicates a slight decrease in the loop pressure in response to a decrease in temperature. Point B is a critical point which indicates the rupture of Metastability. From B-C, an increase in the rate of pressure drop with temperature is an indication that gas is being greatly consumed by spontaneously and rapidly hydrates formation (free CO_2 gas is being encaged in the hydrate). From point C-D, with continuous cooling, hydrate formation continuous and the formation process slows down (the change slope of the pressure is very small).

At point D, cooling is over, formation of hydrate stops. D-E, the loop was heating in order to dissociate hydrate slurry. The temperature starts to increase, however the hydrate dissociation did not start immediately after the loop began warming up. The slight increase of pressure was due to expansion of hydrate. At a certain temperature, the increase in pressure becomes more rapid indicating the start of the hydrate dissociation. Point F marks the end of the experiments where hydrate dissociates completely. Our measurement has very good agreement with the experimental results of Edmonds *et al* 1998 in figure 29.

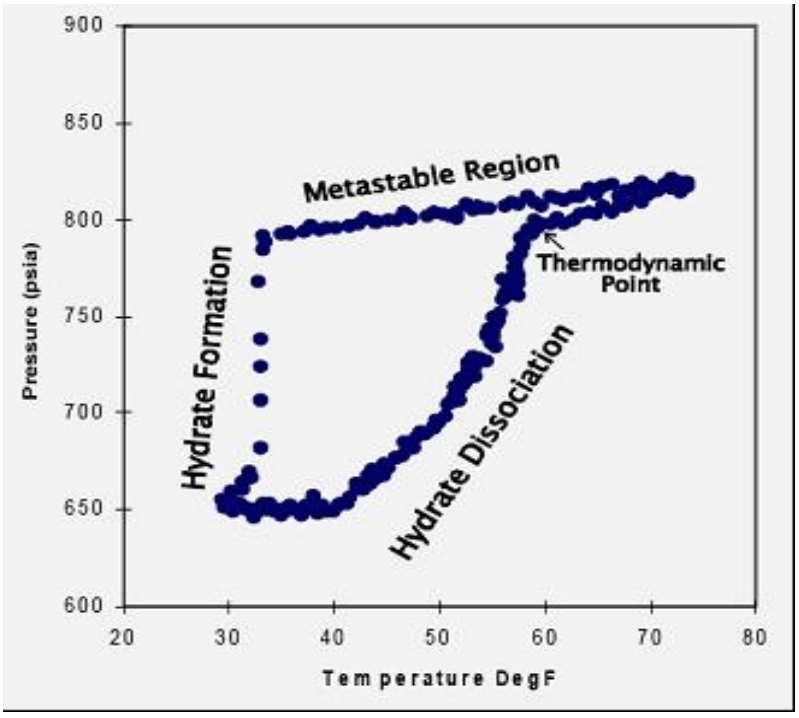

Fig.29: Typical experimental results of hydrate formation and dissociation (source: Edmonds *et al* 1998)

7.6 Hydrate Slurry Stability Experiment

About 32 kg of water in the secondary loop was cooled down to 1°C simultaneously by two chillers. Afterwards, about 3 kg CO_2 gas was injected into the water in several times to form CO_2 hydrate slurry. The final pressure of loop was about 35 bar. When the experimental conditions reached steady state, pressure, temperature and velocity of CO_2 hydrate slurry were maintained at 36 bar, 1.2°C and 1.44 m/s respectively. Density of CO_2 hydrate slurry was examined for almost 12 hours to judge the stability.

Density is looked as an important indicator to judge the stability of CO_2 hydrate slurry. If CO_2 hydrate slurry undergoes the dissociation, density will decrease. Fig.30 shows the density evolution of CO_2 hydrate slurry during 10.5 hours system running period after hydrate formation was completed and in steady state. We can see density of CO_2 hydrate slurry only slightly decreased at the end of experiment. Density was held around 1022 kg/m^3, which corresponds to almost 38 % solid mass fraction. Density remains relatively constant meaning that the CO_2 hydrate slurry displayed good stability under such conditions.

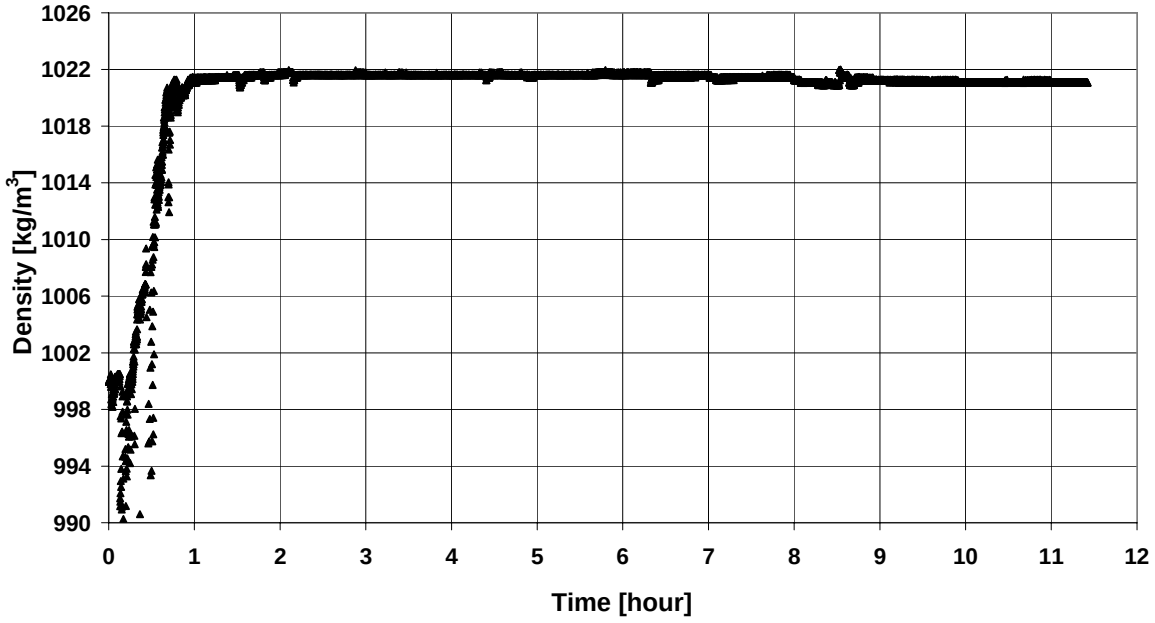

Fig.30: Density evolution of CO_2 hydrate slurry during the stability test

7.7 Relation of Pressure Drop and Mean Velocity

Flow properties of different solid mass fraction of hydrate slurry were studied. The largest hydrate mass fraction in the experiments is 45%. The hydrate mass fraction is denoted as $x_{CO_2 Hydrate}$. The pressure drop over the entire heat exchanger between the negative and positive side of the differential pressure transmitter was measured at a range of mean slurry velocities from 0.5 to 1.5m/s and several solid mass fractions. Fig.31 presents these heat exchanger pressure drops as functions of the mean slurry velocity for several hydrate mass fractions. As it is seen, for each mass concentration, the pressure drops increase with the increasing of mean velocities; the pressure drop is found to increase with increasing mass loading due to particle-wall friction forces. It was observed that for each solid loading, the pressure drop dependence on the flow velocity could approximately be fitted to a quadratic law, as is normal in turbulent flow. The pressure drops increase quickly when the hydrate mass concentration reaches as large as 34%, for such high solid mass fractions, the pressure drop curves are observed to start from a high value at the lowest test velocity;

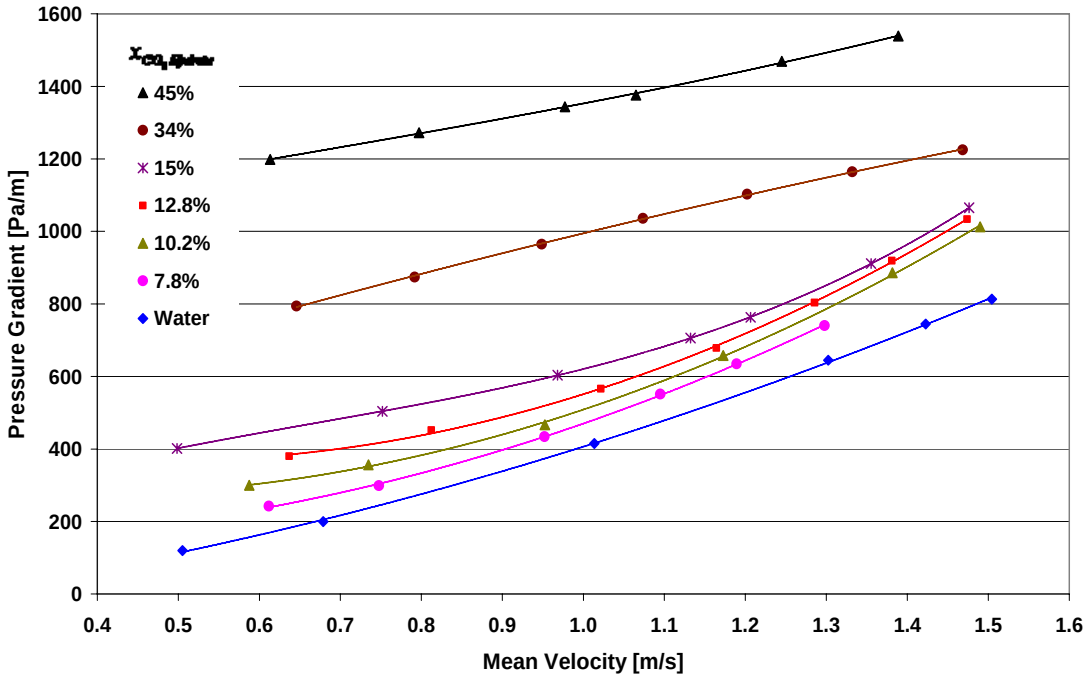

Fig.31: Heat exchanger pressure drop measurements as functions of the mean slurry velocity for several hydrate mass fractions

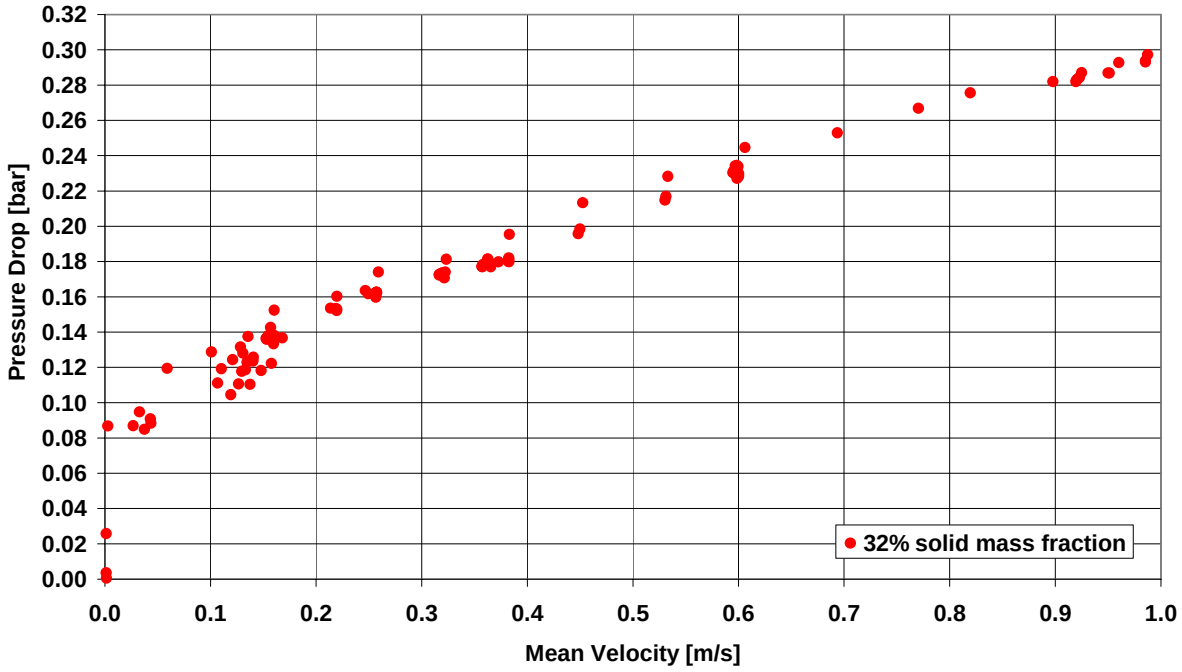

Fig. 32: The pressure drop on heat exchanger at the mean velocity approaching to zero

Figure 32 shows the results of examination of the pressure drop of CO_2 hydrate slurry (about 32% solid mass fraction) on heat exchanger at lowest velocity. When the mean velocity approached to zero, we find pressure drops on heat exchanger was not zero. Such fluid

behaviour can be explained in terms of yield stress (often seen for suspensions) caused by inter-particle cohesive forces. The yield stress is defined in the literature (Darbouret et al., 2005) as the wall shear stress value at the shear rate around zero. For a straight pipeline, the yield stress can be calculated from the balance equation between the wall friction force and the force due to pipeline pressure drop given by:

$$\tau_1 = 0.25 \cdot D \cdot \frac{\Delta p_i}{L_{lam}} \tag{97}$$

where τ_1 is the yield stress, D is the pipe diameter, $\frac{\Delta p_i}{L_{lam}}$ is the pressure gradient at the point of incipient flow where the flow is laminar.

7.8 Heat Transfer Coefficient of CO_2 hydrate slurry

As CO_2 hydrate slurry is a kind of phase change material slurry. It was difficult to obtain the exact value of the local average temperature when the melting of CO_2 slurry particles happens at any position of the pipes and the temperature distribution is not uniform in the heat exchanger. Besides, the effective specific heat of CO_2 hydrate slurry is unknown. Hereby, in this study, we only focus on the calculation of heat transfer coefficient of CO_2 hydrate slurry at steady state in which CO_2 hydrate slurry is homogeneous, temperature, pressure, viscosity, density and the effective specific heat are held at constants. For the case of hydrate slurry density 1019.4 kg/m^3 (15% solid mass fraction), at pressure 36.6 bar, with velocity of 1.476 m/s, delta temperature between inlet of heat exchanger and outlet of heat changer was 0.14°C. Energy balance and log mean temperature approach can be applied to hydrate slurry side and coolant with difference of 3% from previous water test. On the heat exchanger, D_i=0.0297m, D_o=0.0337m. D'=0.0443m, D_c =0.0483; L=22.04m;

The convection coefficient of the CO_2 hydrate slurry of forced flow is given by the following equation

$$h_{Hy} = \frac{1}{\frac{D_i}{D_o}\left[\frac{1}{U} - \frac{\ln(D_o/D_i)}{2 \cdot k} D_i - \frac{1}{h_c}\right]} = 3658 \text{ W/m}^2\text{.K} \tag{98}$$

h_{Hy} is almost double value of h_c. This is different with water test in which $h_{Hy} \approx h_c$. We argue that the heat transfer capacity of the hydrate slurry was greatly enhanced by the formed hydrate solid particles.

To valid this assumption, same amount of Water, unsaturated CO_2 solution and saturated CO_2 solution (CO_2 hydrate slurry) were cooled down at the same cooling speed from 9°C to 0.5°C by two chillers respectively.

Table9. Heat transfer coefficients and overall heat transfer coefficient

Parameters	Coolant
D_h (m)	$D_h = D' - D_o$ $\quad D_h = 1.06 \times 10^{-2}\, m$
$\dot{m}$ (kg/s)	0.943
Cp (J/kg.K)	3669.4
Re_{Dh}	$\mathrm{Re}_{Dh} = \frac{4 \cdot \dot{m}}{\mu_o \cdot \pi \cdot (D' + D_o)}$, $\mathrm{Re}_{Dh} = 2992$, turbulent flow
A (m^2)	2.333
μ (Pa/s)	0.005145
λ (W/m.K)	0.476
Pr	$\mathrm{Pr} = \frac{\mu . C_p}{\lambda}$, $\mathrm{Pr} = 39.7$
Nu_{Dh}	$\mathrm{Nu}_{Dh} = \frac{\left(\frac{f}{8}\right) \cdot (\mathrm{Re}_{Dh} - 1000) \cdot \mathrm{Pr}}{1 + 12.7 \bullet \left(\frac{f}{8}\right)^{\frac{1}{2}} \cdot (\mathrm{Pr}^{\frac{2}{3}} - 1)}$, N_{Dh}=40.2 $f = \left[0.79 \ln(\mathrm{Re}_{Dh}) - 1.64\right]^{-2}$, f=0.0456
h ($W/m^2.K$)	$h = \frac{\lambda Nu_{Dh}}{D_h}$, $h_c = 1807$
T (°C)	T_{hi}=1.24, T_{ho}=1.11, T_{ci}=0.71, T_{co}=0.95
R	$R = \frac{T_{hi} - T_{ho}}{T_{co} - T_{ci}}$, R=0.5464
P'	$P' = \frac{T_{co} - T_{ci}}{T_{hi} - T_{ci}}$, P'=0.4442
P'R	$P' \cdot R = \frac{T_{hi} - T_{ho}}{T_{hi} - T_{ci}}$, $P' \cdot R = 0.2427$
U ($W/m^2.K$)	$U = \frac{\dot{Q}}{\Delta T_{LM} \cdot A} = \frac{\dot{m}_h \cdot c_{p_h} \cdot (T_{hi} - T_{ho})}{(T_{hi} - T_{ci}) \cdot \frac{P' \cdot (R-1)}{\ln\left[\frac{1-P'}{1-P' \cdot R}\right]}} \cdot \frac{1}{\pi \cdot D_o \cdot L}$, **U=1011**

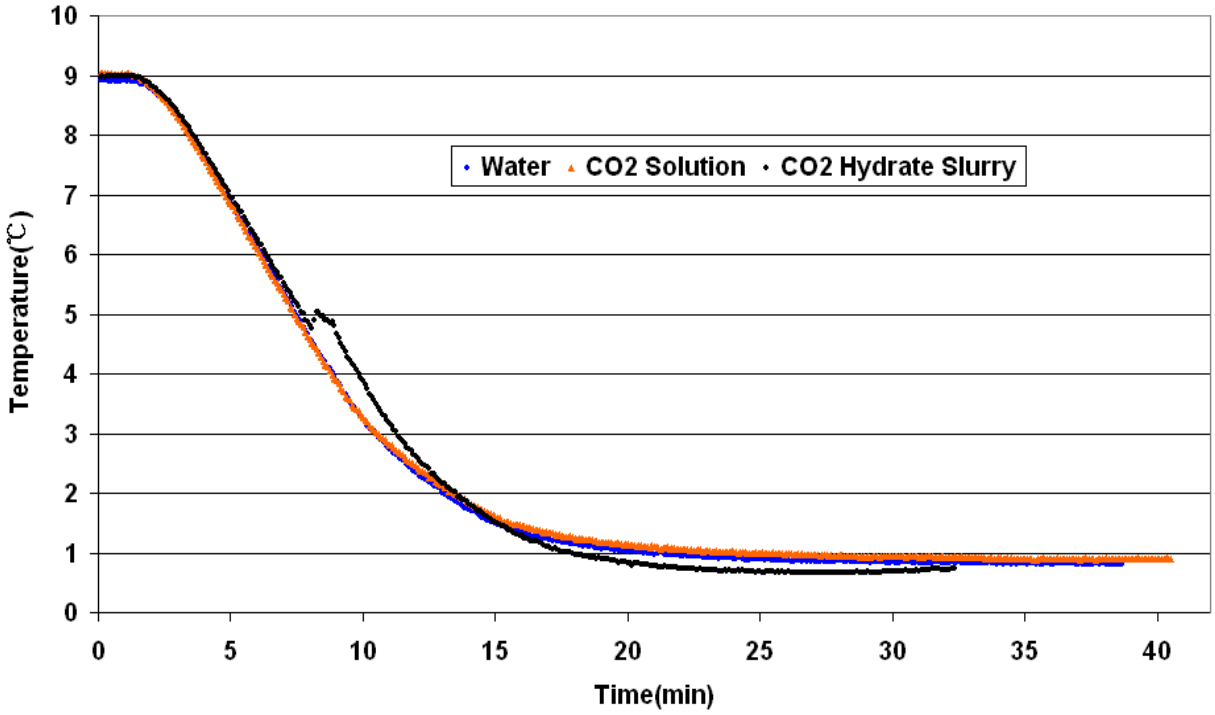

Fig.33 Comparisons of cooling history between water, unsaturated CO_2 solution and CO_2 hydrate slurry

Figure 33 shows the temperature history of three different fluids. Water and unsaturated CO_2 solution (injected CO_2 gas amount was about 1.075 kg) have quite similar cooling history. Their temperatures drop sharply from 9°C to 1.4°C within 17 minutes. Afterwards, temperature curves of water and unsaturated CO_2 solution had a slight decrease and were almost constant when they approached the 0.5 °C. Figure 33 also reveals the temperature of saturated CO_2 solution (injected CO_2 gas amount was about 1.815 kg) drops sharply from 9 ^{o}C to 4.7 °C within 8 minutes as well as water and unsaturated CO_2 solution. Within this period, due to temperature decrease, the saturated CO_2 solution became supersaturated and supersaturation is the driving force of hydrate formation. Hydrates began to form immediately in the solution. As the formation of hydrates is an exothermic process, a large amount of heat was released to the sealed loop in a very short time. Consequently, the two chillers were not able to respond fast enough to such sudden chemical reaction and temperature of the hydrate slurry jumped to 5 °C in less than 15 seconds. Afterwards, due to the large heat capacity of water in this fluid continuous systems and continuous cooling of two chillers, heat of hydrate formation can efficiently dissipate in the water phase, fluid temperature began to drop down sharply. After minutes 15, it is very obvious that CO_2 hydrate slurry was much easier to approach 0.5°C with larger temperature gradient than that of water and unsaturated CO_2 solution at the same cooling rate. We confirmed that CO_2 hydrate slurry has better heat transfer than water and unsaturated CO_2 solution.

8. Conclusions

Based on previous studies, a comprehensive kinetic study of CO_2 hydrates formation and growth was conducted. A general expression is derived for the supersaturation for crystallization of one-component gas hydrates in aqueous solutions. The supersaturation is the driving force of the process, since it represents the difference between the chemical potentials of a hydrate building unit in the solution and in the hydrate crystal. Expressions for the supersaturation are obtained for solutions supersaturated in isothermal or isobaric regime. The results obtained are applied to the crystallization of hydrates of one-component gases.

The kinetics of nucleation of one-component gas hydrates in aqueous solutions are analyzed. The size of the hydrate nucleus and the work for nucleus formation are determined as functions of the supersaturation $\Delta\mu$. Expressions for the stationary rate J of hydrate nucleation are derived. These expressions describe the $J(\Delta\mu)$ dependence for homogeneous nucleation and for heterogeneous nucleation at the solution/gas interface or on solid substrates and nucleation-active micro-particles in the solution.

The solid mass fraction of CO_2 hydrate slurry was determinated in this study.

Prior to study CO_2 hydrate slurry, water tests were performed on the system in the aspects of density, dynamic viscosity, pressure drop, energy balance and heat transfer coefficients. Water test results on the new test rig have shown the measurement device were very accurate and reliable. We find the heat transferred between coolant and water in the double tube heat exchanger is well energy balanced and heat loss is within 3 %.

By using CCD camera, we confirmed that CO_2 hydrate formation process takes place within a few seconds at positive temperature when suitable formation conditions are satisfied. Fast hydrate formation means an efficient energy-saving is available considering CO_2 hydrate slurry as a kind of refrigerant**.**

The experimental results have shown that the apparent viscosity and fluid density change can also be good indicators for knowing the hydrate formation besides pressure and temperature. We argue in the induction period and the beginning of hydrate nucleation, solution viscosity will increase while the growth of the hydrate crystals will slightly decrease the apparent viscosity. The apparent dynamic viscosity of CO_2 hydrate slurry was about 3.4 mPa.s when the solid mass fraction reached about 45%. We find that CO_2 hydrate solid contributes only slightly to the viscosity increase resulting in excellent pump ability regarding power consumption even for a very high density fluid.

The results have shown that hydrate creation through the heat exchanger by super cooling of the saturated CO_2 solution is feasible. Continuous CO_2 hydrate slurry formation and dissociation by heat exchanger was proved to be feasible. Higher solid fraction is expected to obtain if we reduce the reaction water amount and increase the injected gas amount.

CO_2 hydrate slurry displayed very good stability at steady state during 11.5 hours running test. Longer stability period should be expected if the running conditions are maintained.

The pressure drop over the entire heat exchanger was investigated. The pressure drops increase with the increasing of mean velocities and mass concentrations. For high solid mass fractions, the pressure drop curves are observed to start from a high value at the lowest test velocity.

Base on energy balance, we estimated the heat transfer coefficient of CO_2 hydrate slurry at steady state. We argue that the heat transfer capacity of the hydrate slurry was greatly

enhanced due to the formed hydrate solid particles. Experimental results have confirmed the local heat transfer capacity of the CO_2 hydrate slurry was greatly promoted by the formed hydrate solid particles.

9. Outlook

Three main issues will be focused in the future work. One is by using CO_2 membrane techniques to design of the gas/liquid separation system to separate CO_2 gas and CO_2 solution during the hydrate dissociation process in order to promote heat transfer coefficient; another one is development of a simple and special device which can drive the separated CO_2 back into the CO_2 solution. The third target is to develop a simple phase filed model to simulate the process of CO_2 hydrate formation by cooling the saturated CO_2 solution under static conditions in cooperation with ASCOMP.Ltd.

10. Acknowledgements

We are very grateful to the GEBERT RÜF STIFTUNG of Switzerland for their financial support.

11. References:

Adamson, A.W., Physical Chemistry of Surfaces, Wiley, New York, 1982.

Anderson, Graydon K., Enthalpy of dissociation and hydration number of carbon dioxide hydrate from the Clapeyron equation, *J. Chem. Thermodynamics*, 35 (2003) 1171–1183

Apfel, R.E., J. Chem. Phys. 54 (1971) 62.

Aya, I., Yamane, K. and Narial, H, Solubility of CO_2 and density of CO_2 hydrate, AT 30 MPa, *Energy* Vol. 22, No. 2/3, pp. 263-271, 1997

Aya, I., Yamane, K. and Yamada, N., "Effect of CO2 concentration in water on the dissolution rate of its clathrate", In: Proceedings of The International Symposium on CO2 Fixation and Efficient Utilization of Energy, pp. 351–360 Tokyo, Japan, 1993

Ayel, V., Lottin, O., Peerhossaini, H., Rheology, flow behaviour and heat transfer of ice slurries: a review of the state of the art. *International Journal of Refrigeration*, 2003; 26(1):95–107.

Bel, O., Lallemand, A., Study of a two phase secondary refrigerant intrinsic thermophysical properties of an ice slurry, *International Journal of Refrigeration*, 1999, 22(3):164–74.

Bishnoi, P.R. and Natarajan, Formation and Decomposition of Gas Hydrates, *Fluid Phase Equilibria* 117 (1996) 168-177

Circone S., Stern L. A., Kirby S. H., Durham W. B., Chakoumakos B. C., Rawn C. J., Rondinone A. J. and Ishii Y. (2003) CO_2 hydrate: Synthesis, composition, structure, dissociation behavior and a comparison to structure I CH4 hydrate. *J. Phys. Chem.* B 107 (23), 5529–5539.

Darbouret, M., Cournil, M., Herri, J.-M., Rheological study of TBAB hydrate slurries as secondary two-phase refrigerants, *International Journal of Refrigeration*, Volume 28, Issue 5, August 2005, Pages 663-671

Delahaye, A., Fournaison, L., Marinhas, S., Martínez, M.C., Rheological study of CO2 hydrate slurry in a dynamic loop applied to secondary refrigeration, *Chemical Engineering Science* 63 (2008) 3551 -- 3559

Denbigh, K., the Principles of Chemical Equilibrium, Cambridge University Press, Cambridge, 1971.

Duan, Z., Hu, J., Li, D. and Mao, S., 2008, *Density of the CO_2-H_2O and CO_2-H_2O-NaCl Systems Up to 647 K and 100 MPa*, Energy and Fuels, 22(3), p. 1666-1674.

Duan, Z., Sun, R., Zhu, C. and Chou, I-M, 2006, An Improved Model for the Calculation of CO_2 Solubility in Aqueous Solutions Containing Na^+, K^+, Ca^{2+}, Mg^{2+},Cl^- and SO_4^{2-}, Marine Chemistry, 98, p. 131-139.

Edmonds, B., Moorwood, R. A. S. and Szczepanski, R., Hydrate Update GPA Spring Meeting, Darlington, May 1998

Englezos, P., Kalogerakis, N.E., Dholabhai, P.D., Bishnoi, P.R., 1987a. Kinetics of formation of methane and ethane gas hydrates. Chemical Engineering Science 42, 2647–2658.

Firoozabadi, A., Thermodynamics of Hydrocarbon Reservoirs, McGraw-Hill, New York, 1999.

Fleyfel, F., Song, K.Y., Kook, A., Martin, R. and Kobayashi, R., Annals of New York Academy of Science, 715 (1994).

Fournaison, L., Delahaye, A. and Chatti, I., Petitet, J-P., CO_2 hydrates in Refrigeration Processes, *Ind.Eng.Chem.Res,* 2004, 43, 6521-6526

Gborigi , M., Riestenberg , D., Lance , M., McCallum , S., Atallah , Y., Tsouris, C., Raman spectroscopy of a hydrated CO2/water composite, Journal of Petroleum Science and Engineering 56 (2007) 65–74

Hironori, H., Taro, K., Takeshi, K., Yoshitaka, Y., Yoshihiro, O., Kotaro, O., Kiyoshi, H., Effect of CO2 Concentration and Raman analysis of Gas Hydrate Components. Fundamental study on the formation and dissociation of CO2 gas hydrate, (2nd Report), *Journal of the Mining and Materials Processing Institute of Japan*, Vol.117**,** No.9, pp.731-735 (2001)

Holder, G., Mokka, L., Warzinski, R., Formation of Hydrates from Single-Phase Aqueous Solutions and Implications for Oceanic Sequestration of CO_2, the American Chemical Society Division of Fuel Chemistry in the Preprints of the Spring 2001 National Meeting in San Diego, California

Hu, J., Sari, O., Eicher, S., Homsy, P., Thermo Physical and Flow Properties of CO_2 Hydrate Slurry**,** w1-05, proceedings of 8th IIR Gustav Lorentzen Conference on Natural Working Fluids

Jarvis, T.J., Donohue, M.D., Katz, J.L., J. Colloid Interface Sci. 50 (1975) 359.

Kashchiev, D., Nucleation: Basic Theory with Applications, Butterworth-Heinemann, Oxford, 2000.

Kashchiev, D., Firoozabadi, A. J., Crystal Growth 241 (2002a) 220.

Kashchiev, D., Firoozabadi, A., 2002b. Nucleation of gas hydrates. Journal of Crystal Growth 243, 476–489.

Krotov,V.V., Rusanov, A.I., Physicochemical Hydrodynamics of Capillary Systems, Imperial College Press, London, 1999.

Langer, J., Models of pattern formation in first-order phase transitions, in: G. Grinstein, G. Mazenko (Eds.), Directions in Condensed Matter Physics, World scientific, Singapore, 1986, pp. 165–185.

Li Dong-Liang, Liang De-Qing, Fan Shuan-Shi, Li Xiao-Sen, Tang Liang-Guang, Huang Ning-Sheng, In situ hydrate dissociation using microwave heating: Preliminary study, *Energy Conversion and Management* 49 (2008) 2207–2213

Lin, W., Delahaye, A.and Fournaison, L., Phase equilibrium and dissociation enthalpy for semi-clathrate hydrate of CO2 + TBAB, *Fluid Phase Equilibria*, Volume 264, Issues 1-2, 1 March 2008, Pages 220-227

Makogon,Y.F., Hydrates of Hydrocarbons, Pennwell, Tulsa, 1997.

Marinhas, S., Delahaye, A., Fournaison, L., Dalmazzone, D., Furst, W., Petitet, J.-P., 2006. Modelling of the available latent heat of CO2 hydrate slurry in an experimental loop applied to secondary refrigeration. *Chemical Engineering and Processing* 45, 184--192

Matsumoto, K., Namiki, Y., Okada, M., Kawagoe, T., Nakagawa, S., Kang, C., Continuous ice slurry formation using a functional fluid for ice storage, *International Journal of Refrigeration*, 2004; 27(1):73–81.

Miyazaki, T., Takeuchi, A., Koyama, T., Computer simulations of the phase decomposition on Cu–Co binary alloys based on the non-linear diffusion equation, J. Mater. Sci. 27 (1992) 2444–2448.

Moore, G.R., Ph.D. Thesis, University of Wisconsin, Madison, 1956.

Morgan, J J., Blackwell, V., Johnson, D., Spencer, D. and North, W.J, Hydrate Formation from Gaseous CO_2 and Water, *Environ. Sci. Technol*. 1999, 33, 1448-1452

Natarajan, V., Ph.D. Thesis, University of Calgary, Calgary, 1993.

Natarajan,V., Bishnoi, P.R., Kalogerakis, N., Chem. Eng. Sci. 49 (1994) 2075.

North, W. J., Blackwell, V. and Morgan, J.J., Studies of CO_2 hydrate formation and dissociation, *Environ. Sci. Technol*, 1998, 32, 676-681

Ogoshi, H. and Takao, S., Air-Conditioning System Using Clathrate Hydrate Slurry, JFE GIHO, No. 3 (Mar. 2004), p. 1–5

Ota Masahiro and Ferdows Mohammad, Monte Carlo Approach to Structure and Thermodynamic Property of CO_2 Hydrate, Series B, Vol.48, No.4, 2005, Special Issue on Advanced Combustion Technology in Internal Combustion Engines pp.802-809

Oyama, H., Ebinuma, T., Shimada, W., Takeya, S., Nagao, J., Uchida, T. and Narita, H., 2003, *An Experimental Study of Gas-Hydrate Formation by Measuring Viscosity and Infrared Spectra*, Can. J. Phys. , **81**, p. 485-492.

Oyama, H., Shimada, W., Ebinuma, T., Kamata, Y., Takeya, S., Uchida, T., Nagao, J. and Narita, H., Phase diagram, latent heat, and specific heat of TBAB semiclathrate hydrate crystals, *Fluid Phase Equilibria*, Volume 234, Issues 1-2, 28 July 2005, Pages 131-135

Prausnitz, J.M., Lichtenthaler, R.N., de Azevedo, E.G., Molecular Thermodynamics of Fluid-Phase Equilibria, Prentice-Hall, Englewood Cliffs, 1986.

Sari, O., Hu, J., Brun, F., Erbeau, N., Homsy, P., Logel, J-C., In-situ Study of the Thermal Properties of Hydrate Slurry by High Pressure DSC, ICR07-B1-1611, International Congress of Refrigeration, 2007, Beijing, China

Skovborg, P. and Rasmussen, P., A mass transport limited model for the growth of methane and ethane gas hydrates, *Chemical Engineering Science* , 42, 11, 1131-1143, 1994.

Solan, E.D., Clathrate Hydrates of Natural Gases, Marcel Dekker Inc., New York, 1, 1991

Sloan, E.D., 1998. Clathrate Hydrates of Natural Gases, second ed. CRC.

Span, R., Wagner, W., J. Phys. Chem. Ref. Data 25 (1996) 1509.

Stackelberg, M.V. and Müller. H.R., On the structure of gas hydrates, *J.Chem.Phys*., 19, 1319-1320

Takenouchi, S. and Kennedy, G.C., *Journal of Geology*, Vol. 73, 883, 1965

Takeya, S., Hori, A., Hondoh, T., Uchida, T., 2000. Freezing-memory effect of water on nucleation of CO2 hydrate crystals. Journal of Physical Chemistry B 104, 4164–4168.

Tanasawa, I. and Takao, S., Low-temperature storage using clathrate hydrate slurries of tetra-n-butylammonium bromide: thermophysical properties and morphology of clathrate hydrate crystals. In: Fourth international conference on gas hydrates. Yokohama, Japan; 2002. p. 963–7.

Tanino, M., Kozawa, Y., Ice–water two-phase flow behavior in ice heat storage systems. *International Journal of Refrigeration*, 2001, 24(7):639–51.

Teng, H., Yamasaki, A., Shindo, Y., Stability of The Hydrate Layer Formed on the Surface of a CO_2 Droplet in High-Pressure, Low-Temperature Water, *Chemical Engineering Science*, Vol. 51, No.22, pp.4979-4986, 1996

Teng, H., Yamasaki, A., Shindo, Y., The Fate of Liquid CO_2 Disposed of in the Ocean, Energy Vol. 21, No.9, pp. 765-774, 1996

Uchida, T., Ohmura, R., Nagao, J., Takeya, S., Ebinuma, T. and Narita, H., 2003, *Viscosity of Aqueous CO_2 Solutions Measured by Dynamic Light Scattering*, J. Chem. Eng. Data, **48**, p. 1225-1229.

Uchida, T., Takagi, A., Hoirano, T., Narita, H., Kawabata, J., Hondoh, T. and Mae, S., Measurements on Guest-Host Molecular Density Ratio of CO2 and CH4 Hydrates by Raman Spectroscopy, 2nd Int. Conf. Natural Gas Hydrates, Toulouse, France, pp.335-339, 1996

Uchida, T., Takagi, A., Kawarata, J., Mae, S. and Hondoh, T., Raman : Specrroscopic Analyses on the growth process od CO2 hydrates , Energy Convers. Mgmt Vol. 36, No. 6-9, pp. 547-550, 1995

Udachin, K. A., Ratcliffe C. I. and Ripmeester J. A., (2001) Structure, composition and thermal expansion of CO2 hydrate from single crystal X-ray diffraction measurements. *J. Phys. Chem.* B 105 (19), 4200–4204.

Udachin, K.A., Ratcliffe, C.I. and Ripmeester, J.A., Single Crystal Diffraction Studies of Structure I, II and H Hydrates: Structure, Cage Occupancy and Composition, *Journal of Supramolecular Chemistry* 2 (2002) 405–408

Unruh, C. H. and Katz, D.L., Gas hydrates of carbon dioxide-methane mixtures, *Pet.Trans. AIME* 186, 83-86, 1949.

Wagner, W. and Pruss, A., 2002, The IAPWS Formulation 1995 for the Thermodynamic Properties of Ordinary Water Substance for General and Scientific Use, J. Phys. Chem. Ref. Data, 31(2), p. 387-535.

Watson, J.T.R., Basu, R.S. and Sengers, J.V., 1980, *An Improved Representative Equation for the Dynamic Viscosity of Water Substance*, J. Phys. Chem. Ref. Data, 9(4), p. 1255-1290.

Zhong, Y., Rogers, R.E., 2000. Surfactant effects on gas hydrate formation, *Chemical Engineering Science* 55, 4175–4187.